Analyzing the Impacts of Discretization and Meshing in Numerical Simulation of
Unconventional Reservoirs

by

Ziming Xu

A thesis submitted in partial fulfillment of the requirements for the degree of

Master of Science

in

Petroleum Engineering

Department of Civil and Environmental Engineering
University of Alberta

Abstract

The discrete fracture network (DFN) model is widely used to simulate and represent the complex fractures occurring over multiple length scales. However, computational constraints often necessitate that these DFN models be upscaled into a dual-porosity dual-permeability (DPDK) model and discretized over a corner-point grid system, which is still commonly implemented in many commercial simulation packages. Many analytical upscaling techniques are applicable, provided that the fracture density is high, but this condition generally does not hold in most unconventional reservoir settings. A particular undesirable outcome is that connectivity between neighboring fracture cells could be erroneously removed if the fracture plane connecting the two cells is not aligned along the meshing direction.

In this work, a novel scheme is proposed to detect such misalignments and to adjust the DPDK fracture parameters locally, such that the proper fracture connectivity can be restored. A search subroutine is implemented to identify any diagonally adjacent cells whose connectivity has been erroneously removed during the upscaling step. A correction scheme is implemented to facilitate a local adjustment to the shape factors in the vicinity of these two cells while ensuring the local fracture intensity remains unaffected. The results are assessed in terms of the stimulated reservoir volume calculations, and the sensitivity to fracture intensity is analyzed.

The method is tested on a set of tight oil models constructed based on properties representative of the Bakken formation. Simulation results of the corrected, upscaled models are closer to those of DFN simulations. There is a noticeable improvement in the production after restoring the connectivity between those previously disconnected cells. The difference is most significant in cases with medium DFN density, where more fracture cells become disconnected after upscaling

(this is also when most analytical upscaling techniques are no longer valid); in some 2D cases, up to a 22% difference in cumulative production is recorded. The method is subsequently applied to simulate fracturing fluid flowback and the effects of non-planar hydraulic fractures. The results show a significant improvement in the restoration of the fracture connectivity and the ensuing fracture fluid recovery efficiency. Ignoring the impacts of mesh discretization could result in an unintended reduction in the simulated fracture connectivity and a considerable underestimation of the cumulative production.

Preface

This thesis is an original work by Ziming Xu. Similar contents as Chapter 3 and Chapter 4 of this thesis can be found in a journal paper for which I am the first author and is currently under review: Xu, Z., & Leung, J. Y., "Analyzing the Impacts of Meshing and Grid Alignment in Dual-Porosity Dual-Permeability Upscaling".

Acknowledgements

First and foremost, I would like to express my deep and sincere appreciation to Dr. Juliana Leung for providing invaluable guidance and support during my research. Without her inspiration and persistent help, the project would not have been accomplished. I am also grateful to Dr. Li, Dr. Liu, and Dr. Jin for coming to my final defense as examining committee members and giving me constructive comments and suggestions.

I would like to extend my gratitude to all the professors who have taught and helped me. In addition, I want to thank all the research members in Dr. Leung's research group whom I worked with. I would also like to thank all the people who have ever encouraged and helped me during my MSc study.

Finally, I wish to acknowledge the support and great love of my family. They kept me going on and this work would not have been possible without their input.

Table of Contents

List of Tables

List of Figures

List of Symbols

a = Preexising fracture length

A_m = Fracture area, m^2

B = Formation factor, bbl/STB

e_m = Aperture, m

E = Flowback recovery

$\boldsymbol{F}$ = Fracture tensor

$\boldsymbol{F}_{trace}$ = Trace of the fracture tensor

$\boldsymbol{k}_f$ = Fracture permeability tensor, md

k_m = Intrinsic fracture permeability, m2

$\boldsymbol{k}_m$ = Matrix permeability, md

k_{ro} = Relative permeability of oil

K_I = Stress intensity factor of opening mode

K_{II} = Stress intensity factor of shear mode

L = Fracture spacing, m

$\boldsymbol{n}$ = Unit normal vector of fracture surface

p = Pressure, Pa

P = Fluid pressure inside fracture, Pa

P_{32} = fracture intensity, L^2/L^3

$Plunge$ = Plunge angle, degree

q = Source term

$q_{o,mf}$ = Fracture-matrix transfer

R_s = Solution gas-oil ratio, scf/bbl

S = Saturation

t = Time, s

T_m = Transmissivity

$Trend$ = Trend angle, degree

$\boldsymbol{u}$ = Velocity, m/s

V = Bulk volume, m^3

V_f = Volume of fractures, m^3

Greek Symbols

β = Inclination angle, degree

δ_{ij} = Kronecker delta

λ = Interporosity flow parameter

μ = Viscosity, Pa·s

φ = Porosity

φ_f = Fracture porosity

Φ = Phase potential, Pa

σ = Shape factor, 1/m^2

σ_H = Maximum horizontal in-situ stress, Pa

σ_h = Mimimum horizontal in-situ stress, Pa

θ_m = Initiation angle, degree

Chapter 1: Introduction

This chapter illustrates the background of unconventional reservoir exploration and some prevalent modeling methods to simulate the flow in the unconventional reservoirs; It also presents the problem statement, research objectives, and thesis outline.

1.1 Background

For years, unconventional reserves were considered uneconomic because of the difficulty of production, but as science develops, more and more unconventional reservoirs become profitable. The sheer size of unconventional reserves redefines the limited oil resources. In tight reservoir development, the main difficulty is their ultra-low permeability, usually below 0.1mD. Hydraulic fracturing as a well-stimulation technique dramatically increasing the reservoir conductivity is essential to all commercial unconventional tight and shale reservoir development. Unlike traditional fracturing that intends to generate a dominant bi-wing fracture, fracturing in low-permeability unconventional reservoirs aims to create a complex fracture system that would maximize the fracture surface areas. Slickwater is injected into the designated layer to create highly conductible pathways that may be connecting with pre-existing or secondary (natural or re-activated) fractures (Liu et al., 2019). The entire fracture network can dramatically increase the productivity of the stimulated region. However, flow simulation for such complex fracture networks remains challenging.

Several approaches for modelling flow in fractured media exist. The dual porosity dual permeability (DPDK) model is the first proposed by Warren and Root (1963) and is still widely

adopted. It treats the matrix and fracture domains as two different continua: fluid flow in each system is simulated separately, and the two continua are connected via a fluid transfer function. It is easy to implement and very computationally efficient. However, conventional DPDK depends on the assumption that the fractures are well connected and densely distributed (Sun et al., 2014). The sugar cube approach lacks detailed descriptions of the fracture geometry and is inadequate to capture the fluid flow in the fractures (Yang, 2018). Also, the DPDK model does not properly calculate flow directions if fracture orientations are misaligned with the model axes (Panfili, 2014).

The discrete fracture model (DFM) can accurately capture the connectivity of fractured reservoirs and resolve the fracture system in greater detail compared to the conventional dual continuum models (Dershowiz et al., 2000). In DFM, fracture elements or planes can be incorporated in either structured or unstructured meshes. Fractures are aligned with the grid blocks' faces, and fracture parameters are assigned to the defined fracture faces. In structured meshing, only orthogonal fractures are typically represented (Wang, 2016). Unstructured meshing, on the other hand, can incorporate fractures in arbitrary orientation using triangle or PEBI grids in the 2D model (Karimi-Fard et al., 2004; Sun and Schechter, 2014) and tetrahedral grids in the 3D model (Hui et al., 2007). DFM simulation with unstructured meshing would offer more accurate predictions because detailed fracture-fracture, matrix-matrix, and fracture-matrix interactions, as well as the ensuing flow response, can be captured. However, unstructured DFM simulation is computationally expensive; hence, it is not widely adopted, particularly in practical field-scale simulation (Moinfar, 2012). Similarly, history-matching using a DFN model is also challenging because updating DFN model parameters and repeating DFN simulations can be very time-consuming (Nejadi et al., 2015).

The embedded discrete fracture model (EDFM) offers a cheaper, more efficient, alternative to DFM simulation. The method was originally proposed by Lee et al. (2001) for simulating flow in

fractures whose length (L) is much larger than the grid size (L_{grid}). Many additional improvements have been made over the years (Li and Lee 2008; Moinfar et al., 2014; Panfili et al., 2014; Fumagalli et al., 2016; Jiang and Younis, 2017; Hajibeygi et al.,2011; Tene et al., 2017 and Ding et al., 2018). The EDFM method does not require unstructured meshing and can be used on a corner-point grid (Dong, 2019). The fracture planes are embedded within the background matrix grid cell. Interactions between individual fracture segments and matrix sub-regions are modelled using a set of non-neighboring connections (NNC) (Xu, 2017). There are four types of NNCs: matrix-matrix connection, fracture-matrix connection, and fracture-fracture connection in a single fracture extending over multiple grid cells, and fracture-fracture connection among multiple intersecting fractures (Xu, 2018). The accuracy and efficiency of the EDFM method, particularly in hydraulically-fractured tight/shale reservoir simulation, have been demonstrated in many studies (Moinfar, 2012; Kumar, 2019; Liu, et al., in press). However, the EDFM method has not been widely incorporated in most commercial simulation software packages; as a result, the DPDK is still the most prevalent method for simulating unconventional reservoirs.

It is common to construct a set of discrete fracture networks (DFN) and upscale them to DPDK models for flow simulation (Dershowitz, 2000; Sarda et al., 2001; Vitel and Souche, 2007; Nejadi et al., 2017; Zhong and Leung, 2020; Sherratt, 2020). Each discrete fracture is explicitly represented in the DFN in a 3D space, where its size and properties (e.g., location, orientation, shape, aperture, length, height, porosity, and permeability) are specified (Wang, 2019). The fracture geometry (or outline of a fracture) can be described by a point set (Hoeink and Stoddard, 2016). Statistical distributions of fracture parameters can be used to generate these DFNs stochastically (Noorishad and Mehran,1982). In such models, fracture properties from DFN are

3

upscaled to equivalent parameters using the upscaling technique (Nejadi, 2017), and the upscaled finite-difference grid is solved by commercial multiphase flow simulators (Sherratt, 2020).

This method best preserves the geological reality of the described fractures for the dual-porosity model. Also, DPDK models are usually more computationally efficient than most DFM approaches for similar vertical layering and areal grid cell sizes (Kumar,2019). Therefore, the implementation of this modelling method can be found in many works (Akram, 2010; Hui, 2013; Panfili, 2014; Ynag, 2018; Kumar, 2019; Vo, 2019; Zhong and Leung, 2020; Nwabia and Leung, 2020).

1.2 Problem Statement

However, upscaling a DFN to its equivalent DPDK model can be challenging. For example, connections between neighbouring fracture cells could be erroneously removed if the fracture plane connecting the two grid cells is not aligned with the grid axes, resulting in a zero flux between the two cells. In unconventional reservoir settings, the permeability of a matrix is very low and the most fluid flow is through the connected fracture network. A disconnected fracture network will lead to an underestimation of the drainage area, diminishing the accuracy of the DPDK simulation result.

This is usually not a problem if the fracture network is dense; however, in many unconventional reservoirs where the secondary fractures are not densely populated, this issue would lead to an underestimation of the fracture network conductivity and affecting the accuracy of the DPDK simulation results. Other authors, including Lee (2001) and Moinfar et al. (2011), also discussed

how DPDK cannot be used to simulate long fractures (L< L_{grid}) that are not aligned orthogonally to the grid axes.

Therefore, we intend to solve the illustrated problem and propose a workflow to fix those erroneously removed DPDK parameters to restore the fracture-connectivity in the DFN upscaled DPDK model. However, identifying and correcting the disconnected fracture grid blocks could be challenging. Firstly, identifying the missing values in the DPDK upscaled parameters is not trivial, especially when the number of fractures in a DFN is in the hundreds or thousands. Secondly, the DPDK model is an upscaled, or effective representation of the original DFN model; two nearby DPDK cells may or may not be connected by one or more fractures. Special care must be exercised when deciding which connections need to be re-established, in order to avoid over-or under-overestimation of the fracture network conductivity. Thirdly, a scheme must be formulated to re-establish the local connections, while preserving the characteristics of fracture distribution locally (e.g., not artificially or unintentionally introducing many additional fractures). In other words, an appropriate strategy must be devised to assign upscaled parameters (fracture permeability, fracture porosity, and fracture spacing) in a consistent manner. It is important that the re-assigned DPDK parameter would restore the local fracture connectivity and without undue influence on the nearby grid blocks.

In addition, there have not been many previous studies analyzing the impacts of fracture properties (e.g., density, length, and orientation) on the upscaling of DPDK model parameters. Studying the effects of these factors on this phenomenon is helpful to understand the limitations of the upscaling method and to emphasize the possible factors affecting the results in the flow simulation.

1.3 Research Objective

This thesis aims to illustrate the impact of this misalignment in the ensuing DPDK simulation results, and propose an innovative method to re-establish that missing connection to restore the local connectivity, and to enhance the accuracy of resultant DPDK models, which entails:

(1) Propose and devise a workflow to identify any diagonally adjacent cells whose connectivity has been erroneously removed from the upscaling process;

(2) Formulate appropriate correction schemes based on the understanding of DPDK flow simulation and upscaling techniques for the fracture parameters to facilitate a local adjustment to the shape factor in the vicinity of these two cells while ensuring the local fracture intensity remains unaffected.

(3) Assess the feasibility and effectiveness of the developed algorithms by upscaling a set of 2D and 3D DFN simulation models into the equivalent DPDK models, which are constructed based on typical properties gathered from the Bakken formation.

(4) Compare the results of these corrected DPDK models to those corresponding to the equivalent EDFM simulations for validation.

(5) Extend the study to the application of flowback analysis and simulation of the non-planar twisted hydraulic fractures to evaluate the influence of mesh misalignment and disconnected fracture connectivity.

(7) Conduct sensitivity analysis to assess the impacts of mesh resolution and certain DFN parameters on the final DPDK model parameters. The objective is to assess how connections

between fractures were retained or removed for different mesh sizes and fracture properties (e.g., fracture density, fracture length, and fracture angle).

1.4 Thesis outline

The thesis consists of eight chapters. The outline of these chapters is provided as follows:

Chapter1 presents the background of shale exploration and multiple modeling methods to simulate the flow in the unconventional reservoir; problems statement and research objectives are also presented.

Chapter 2 presents the literature review including the existing studies and current research status on DPDK model, discrete fracture network and relative upscaling methods.

Chapter 3 presents the methodology including constructing a DPDK model, upscaling a DFN to a DPDK model and the proposed workflow to re-establish the missing connection.

Chapter 4 presents the case study on Bakken formation by upscaling a set of 2D and 3D DFN simulation models into the equivalent DPDK models. Also, in this chapter, the result of the corrected DPDK model is compared to the equivalent EDFM simulations; It also presents a sensitivity analysis assessing the impacts of mesh resolution and certain DFN parameters on the upscaling performance. The impact of fracture density, fracture length, and fracture angle are analyzed in this chapter.

Chapter 5 presents the impact of missing DPDK upscaled parameters on the simulation of flowback. Both the soaking and flowback periods are simulated using a DPDK model. The

predicted water and oil production profiles corresponding to the original and corrected DPDK models are compared.

Chapter 6 assess the impacts of non-planar hydraulic twisted fractures. Once again, the performance of the original DPDK model is compared against that of the corrected model to assess the applicability of the proposed workflow.

Chapter 7 presents the conclusions and contributions of this thesis. Finally, some suggestions for future works are also discussed.

Chapter 2: Literature Review

2.1 Dual Porosity Dual Permeability Model

The use of the dual-continua formula to model naturally fractured reservoirs (NFRs) dates back at least to Warren & Root (1963). The proposed sugar cube model described the reservoir as an overlapped system of fracture and matrix, and the application of shape factor (Barenblatt,1960) provided an idea for solving the uniformly or nonuniformly distributed fractures by using an equivalent model. However, their rudiment of Dual Porosity Single Permeability models (DPSK or DP) constrains a single-phase flow that can only transfer between fracture system in a one-dimensional radial flow. Kazemi (1969) extended Warren and Root's initial implementation to a more complex situation in two dimensions. Then Kazemi et al. (1976) integrated the two-phase flow to the DP model and accounted for imbibition, gravity, relative mobility, and variation in reservoir properties to the model. Later Rossen (1977) improved the instability of the DP model by introducing the semi-implicitly method both for pressure and saturation and considered the hysteresis effect in the matrix-fluid saturations. Thomas et al. (1983) described a highly stable formulation for DP model by using the implicit method for fracture and matrix/fracture flow, and developed a three-dimensional (3D), three-phase model for simulating the flow of water, oil, and gas in a naturally fractured reservoir. In the same year, Blaskovich et al. (1983) illustrated the limitation of the DP model and emphasized the flow could occur within the matrix. Further, they developed the first multicomponent dual-porosity dual-permeability (DPDK) model in the true sense, which formulates fluid flow in each system is simulated separately, and the two continua are connected via a fluid transfer function. Different from the DP model, DPDK enables the flow in the matrix system. Blaskovich introduced his model as having the capability to simulate large

reservoirs and can accurately account for variations in fluid properties and a wide range of secondary porosity and permeability systems. Later, the DPDK model is improved for handling large-scale reservoir simulation problems (Hill and Thomas, 1985). The gravity effect is accounted for and incorporated into a fully implicit model for simulating fluid flow in a naturally fractured reservoir (Sonier et al., 1988). With the development of tight reservoirs, Dual Porosity Dual Permeability (DPDK) simulation models start to be used for field-scale simulation of NFRs (e.g., Uleberg and J. Kleppe, 1996). And DPDK parameters (such as shape factors) can be used as history-matching parameters to provide more accurate simulation results (Gilman, 2003).

Since DPDK models generally lack a detailed description of the fracture, a combined version of the discrete fracture network (DFN) model and the dual porosity concept has been proposed and proved to be more accurate (Dershowitz et al., 2000; Sarda et al., 2002). This method uses DFN for fracture characterization, which integrates the available information from microseismic, well logs, well test, and production data to identify density, length, orientation and other useful parameters to better describe the NFRs (Akram, 2010). The advantages of accuracy and high efficiency make the DFN upgraded DPDK method widely used in industry and research studies.

Van Heel et al. (2008) summarized all the proposed shape factors, emphasized the importance of considering the dominant physical recovery mechanism, and derived a general formula for the shape factor. More sophisticated techniques involving multiple sub-regions were introduced in the DPDK model better capture the complexities of heterogeneous fracture networks (Hui et al. 2013).

2.2 Modeling of Discrete Fracture Network（DFN）

With the development of microseismic monitoring technology, the understanding of the distribution and geometry of hydraulic fractures is deeper. Due to the heterogeneity of reservoirs and the existence of natural fractures of unconventional reservoirs, complex fracture networks are often generated during the hydraulic fracturing stimulation. A simplified fracture model is usually not sufficient to describe the fracture geometry in the unconventional reservoir. Therefore, a discrete fracture network (DFN) is designed to represent the complex fracture geometry and flow paths generated and affected by hydraulic fracturing and is widely used in reservoir modelling frameworks (Wang, 2015). In numerical modelling, DFN describes a system of discrete fractures which can have any position and orientation in a 3D space. DFN assumes planar features and the shapes of the fracture plane are described by the points that define their outline in three dimensions (Hoeink and Stoddard, 2016).

In an explicitly expressed DFN, each fracture's geometry characteristic like shape and size is directly depicted according to the distributions of different fracture parameters; for example, location, orientation, shape, aperture, length, height, porosity, and permeability (Wang, 2019). However, due to the complex physical mechanism of fracture generation, constructing a DFN from microseismic data is challenging (Rutledge et al., 2013). Not only the log image, but the source mechanisms of microseismic events are also usually studied in order to generate reliable DFN models. The DFN can be generated by extracting the fracture geometry from the seismic data using different algorithms (e.g., Yan, et al. 2011; Hu et al., 2014). Several approaches have been published to obtain DFN from microseismic data (Xu, et al., 2009; Xu, et al. 2010; Williams et al., 2010; Cornette, et al., 2012; Yu, et al., 2016; Vavryčuk, 2015; Yu, et al., 2016). Combined with

different logging data, explicit DFN can generate a realistic representation with good visualization of the natural fracture distribution.

2.3 Upscaling Methods

It is illustrated the importance to simulate the DFN by using the DPDK model. However, to accomplish the simulation of DFN from a DPDK flow simulator, the generated DFN needs to be equivalent to the mashed grid, and the process is called upscaling. This method best preserves the geological reality of the described fractures. The upscaled parameters usually include fracture spacing, fracture permeability, and fracture porosity. Fracture spacing describes an averaged distance between the adjacent fractures in a grid cell for different principal planes, and the fracture spacings determine the value of the shape factor which represents a measure of fracture-matrix interaction between the two domains. Fracture permeability illustrates the effective permeability in the principal direction. Fracture porosity is the ratio of the volume of open fractures to the grid block bulk volume.

There are two common upscaling approaches. The first is the analytical method and the second is the flow-based method. Oda's method is the most prevalent analytical method which defines the DFN permeability based on fracture geometry (Bianch and Snow, 1968; Oda, 1985). The detailed derivation of Oda's method for permeability is presented in Chapter 3. Besides, Haridy (2019) modified Oda's model by introducing the connectivity index, crossing index and length ratio to account for the lack of a definition of a connectivity measure and the assumption of infinite fracture length.

While in the flow-based method, fracture permeability is calculated from Darcy's equation by applying a pressure boundary on the grid blocks (Durlofsky, 2005). Originally, flow-based upscaling is one of the methods used for upscaling geological models from fine grids to coarse grids. Durlofsky (2005) applied this method in upscaling the fracture permeability to the DPDK model and achieved a high degree of accuracy in flow simulation. The flow-based upscaling can capture the spatial variation of pressure and saturation in the matrix and provide more accurate upscaled parameters; Thus, it is usually considered superior to analytical upscaling (Elfeel, 2014). Another prevalent flow-based upscaling is the DFM-based upscaling method, also known as the multiple sub-region (MSR) method (Hui, 2013), which is based on the MINC model of Pruess and Narasimhan (1985). Flow-based upscaling is more accurate; however, it is computationally expensive. Analytical upscaling (i.e. Oda's method) is computationally efficient, yet the accuracy for poorly-connected fractures is not guaranteed (Elfeel, 2014). Depending on the application scenario, both upscaling approaches have their advantages. For a field-scale application, the accuracy benefit of flow-cased upscaling is not as significant as the efficiency benefit of analytical Oda's method. This is why the analytical upscaling approach is still the most common method used in the industry.

Chapter 3: Methodology

3.1. DPDK Flow Simulation

The governing equations for a black-oil system based on the control volume finite difference method can be written as Eq. (3.1), where each equation is integrated over a particular control volume (Ertekin et al., 2001). The subscripts w, o, and g represent water, oil and gas. S, B, $\boldsymbol{u}$, q, t, ϕ, and R_s refer to saturation, formation factor, velocity, source term, time, porosity, and solution gas-oil ratio respectively.

$$
\begin{cases}
\dfrac{\partial}{\partial t}(\dfrac{\phi S_w}{B_w}) + \nabla\left(\dfrac{\boldsymbol{u}_w}{B_w}\right) = q_w \\[3mm]
\dfrac{\partial}{\partial t}(\dfrac{\phi S_o}{B_o}) + \nabla\left(\dfrac{\boldsymbol{u}_o}{B_o}\right) = q_o \\[3mm]
\dfrac{\partial(\phi(\dfrac{S_o R_s}{B_o} + \dfrac{S_g}{B_g}))}{\partial t} + \nabla\left(\dfrac{R_s}{B_o}\boldsymbol{u}_o + \dfrac{\boldsymbol{u}_g}{B_g}\right) = q_g
\end{cases}
\tag{3.1}
$$

In the DPDK formulation, each grid cell is divided conceptually into one fracture sub-cell and one matrix sub-cell (Tao, 2016). Thus, three kinds of fluid transfer phenomena can happen in and between the sub-cells, including matrix-matrix transfer, matrix-fracture transfer, and fracture-fracture transfer. Eq. (3.1) is modified to accommodate the exchange between the different media. For example, after incorporating Darcy's law, the oil component conservation equation is re-written as Eq. (3.2) for the flow in the matrix (m) domain and Eq. (3.3) for flow in the fracture (f) domain. (Chen.2006; Cui, 2016).

$$\frac{\partial}{\partial t}\left(\frac{\phi_m S_{o,m}}{B_{o,m}}\right) = \nabla\left(\frac{\boldsymbol{k}_m k_{ro,m}}{\mu_{o,m} B_{o,m}}\nabla\Phi_{o,m}\right) + q_{o,mf}. \qquad (3.2)$$

$$\frac{\partial}{\partial t}\left(\frac{\phi_f S_{o,f}}{B_{o,f}}\right) = \nabla(\frac{\boldsymbol{k}_f k_{ro,f}}{\mu_{o,f} B_{o,f}}\nabla\Phi_{o,f}) - q_{o,fm} + q_{o,f}. \qquad (3.3)$$

In Eq. (3.2) and Eq. (3.3), Φ and m are the phase potential and the viscosity. $\boldsymbol{k}_m$ denotes the matrix permeability, and $\boldsymbol{k}_f$ is the fracture permeability tensor, also called the effective permeability. k_{ro} is the relative permeability of oil. $q_{o,f}$ is the well transfer term (source term). The term $q_{o,mf}$ (or $q_{o,fm}$) is the fracture-matrix transfer term, which can be regarded as another source term to represent flow through the two different media (Cui, 2016):

$$q_{o,mf} = \sigma \frac{k_{ro,t}}{\mu_{o,t} B_{o,t}}(p_m - p_f). \qquad (3.4)$$

σ is the shape factor. The relative mobility should be computed based on upstream weighting (Ertekin et al., 2001). Finally, p is the pressure.

3.2. Construction of DPDK Model from DFNs

The DFN models are generated stochastically, where probability distributions of different fracture parameters are specified (FRACMAN®). Each DFN model is upscaled to an equivalent DPDK model: for each grid block, the equivalent shape factor, fracture permeability, and fracture porosity are defined from upscaling.

3.2.1. Shape Factor

The shape factor σ is primarily a function of the cell geometry and the fracture spacing (or intensity). It is used to describe an idealized fracture-matrix system, which is called the "sugar cube" model shown in Fig. 3.1. The expression Eq. (3.5) was originally proposed by Warren and Root (1963):

$$\sigma = \frac{4n(n+2)}{l^2}, l = \begin{cases} L_x \\ 2L_x L_y / (L_x + L_y) \\ 3L_x L_y L_z / (L_x L_y + L_y L_z + L_z L_x) \end{cases} . \tag{3.5}$$

n is the number of normal sets of fractures, l is a characteristic dimension of the heterogeneous region, L. Each matrix block has the dimension of L_x, L_y, and L_z. Kazemi et al. (1976) proposed a shape factor expression in Eq. (3.6).

$$\sigma = 4(\frac{1}{L_x^2} + \frac{1}{L_y^2} + \frac{1}{L_z^2}) . \tag{3.6}$$

Where σ is the shape factor L_x, L_y, and L_z represent the spacing between fracture planes within the grid cell (i.e., fracture spacing) in x-, y-, and z-directions. Either fracture spacing or the shape factor can be direct inputs to the flow simulation.
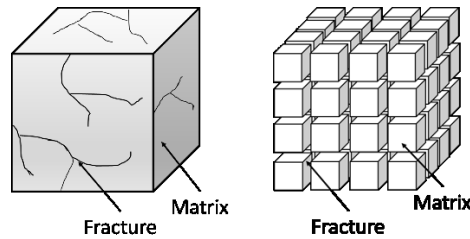
Fig. 3.1. Demonstration of Sugar cube model. (Adapted from Warren and Root, 1963)

3.2.2. Permeability Tensor

Equivalent fracture permeability tensor can be obtained based on either static or flow-based methods. Oda (1985) proposed an analytical method for discontinuous rock masses. The permeability tensor was described as a symmetric second-rank tensor that is dependent on fracture shape, aperture, size, and orientation.

$$k_f = \lambda(F_{trace}\delta_{ij} - F) \ . \tag{3.7}$$

k_f is the equivalent (or effective) permeability tensor (Cottereau, 2010); λ is the interporosity flow parameter (Kazemi, 1969), which is a constant equal to 1/12 if the rock is fully broken up by fractures; δ_{ij} is the Kronecker delta ($\delta_{ij} = 1$ if $i = j$; $\delta_{ij} = 0$ if $i \neq j$); F_{trace} is the trace of the fracture tensor (F), which can be evaluated for a specific grid cell according to Eq. (3.8) (Dershowitz, 2000).

$$F = \frac{1}{V}\Sigma_{m=1}^{M} A_m T_m n_{im} n_{jm} n_{km} \ . \tag{3.8}$$

V is the volume of fractures; M represents the number of fractures within a grid cell and m is the index of summation; A_m is the fracture area; T_m is the transmissivity of the fractures which is equal to the multiplication of e_m and km, where e_m is the aperture and k_m is the intrinsic fracture permeability; n is the unit normal vector of the fracture surface. The equivalent permeability tensor can be further expressed as below in Eq. (3.9), and the detailed derivation is shown in Appendix A.

$$\mathbf{k}_f = \frac{1}{12V}\sum\nolimits_{m=1}^{M} A_m e_m k_m \left\{ \begin{bmatrix} C_{11} & 0 & 0 \\ 0 & C_{22} & 0 \\ 0 & 0 & C_{33} \end{bmatrix} - \right.$$

$$\left. \begin{bmatrix} \sin(Trend_m)\sin(Trend_m) & \sin(Trend_m)\cos(Trend_m) & \sin(Trend_m)\sin(Plunge_m) \\ \sin(Trend_m)\cos(Trend_m) & \cos(Trend_m)\cos(Trend_m) & \cos(Trend_m)\sin(Plunge_m) \\ \sin(Trend_m)\sin(Plunge_m) & \cos(Trend_m)\sin(Plunge_m) & \sin(Plunge_m)\sin(Plunge_m) \end{bmatrix} \right\}$$

$$C_{11} = C_{22} = C_{33} = \sin^2(Trend_m) + \cos^2(Trend_m) + \sin^2(Plunge_m). \tag{3.9}$$

In Eq. (3.9), the trend angle is the clockwise angle between that the fracture normal makes measured clockwise relative to and the north; Plunge angle is the angle between the fracture normal and the x-y plane. It is clear from Eq. (3.9) that the equivalent permeability tensor would be greater than zero as long as there is at least one fracture located within the grid block.

The permeability tensor can also be calculated from other flow-based methods, where different boundary conditions (e.g., periodic or constant pressure) can be imposed on the faces of a grid cell (Haridy, 2019; Durlofsky, 2005). Flow-based upscaling is generally more accurate, but it is also more time-consuming. Therefore, for a full field study, static methods, like Oda's method, is still widely adopted (Ahmed et al., 2014).

3.2.3. Fracture Porosity

Fracture porosity (ϕ_f) is defined as the ratio of fracture volume to the grid block bulk volume (V). The equation can be expressed by (Dershowitz, 2000):

$$\phi_f = \frac{\sum_{m=1}^{M} V_f}{V} = \frac{\sum_{m=1}^{M}(A_m e_m)}{V} = P_{32}e . \tag{3.10}$$

Where M is the number of fractures within a grid cell and m is the index of summation. A_m is the fracture area; e_m is fracture aperture; P_{32} is fracture intensity defined as fracture area per unit volume.

3.3. Proposed Workflow

In cases when the fracture is not aligned with the grid axes, certain fractures in the upscaled DPDK model would become disconnected. An example is shown in Fig. 3.2 (a) – the fracture becomes disconnected in the middle. This error can be possibly explained by the numerical thresholds of the upscaling procedure, where fracture segments within a certain cell (e.g., the red cell) may be ignored if its length is too small. This issue would reduce the overall conductivity of the fracture.

To determine whether certain connections need to be re-established (i.e., re-assigning some fracture parameters to the red cell in Fig. 3.2 (a)), a scanning procedure is formulated. Even if two fracture cells are close to one another, it does not necessarily mean that they belong to a set of connected fractures and be connected. Two examples are shown in Fig. 3.2(b).

Fig. 3.3 outlines the developed workflow; it consists of two parts: identifying and correcting disconnections. Although the method described here can be applied for any fracture shapes and sizes, in this study, only rectangular planar fractures are considered. To simplify our calculations, fractures are idealized as lines in 2D and planes in 3D.
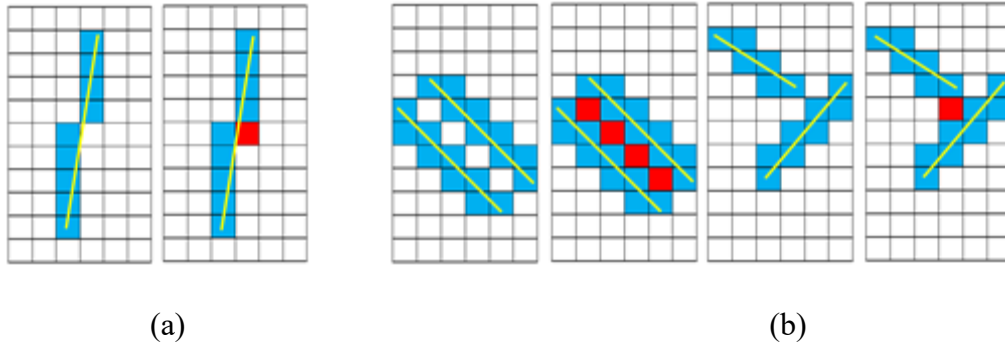
Fig. 3.2. (a) A diagram of a misaligned fracture and how it is disconnected after the upscaling process (the missing red cell is needed to connect the entire fracture segment). (b) Illustration of how nearby fracture cells should not be connected (the red cells are legitimately missing here). Yellow lines are fractures, blue grid blocks are the place where the fracture properties are non-zero after upscaling to a DPDK model.
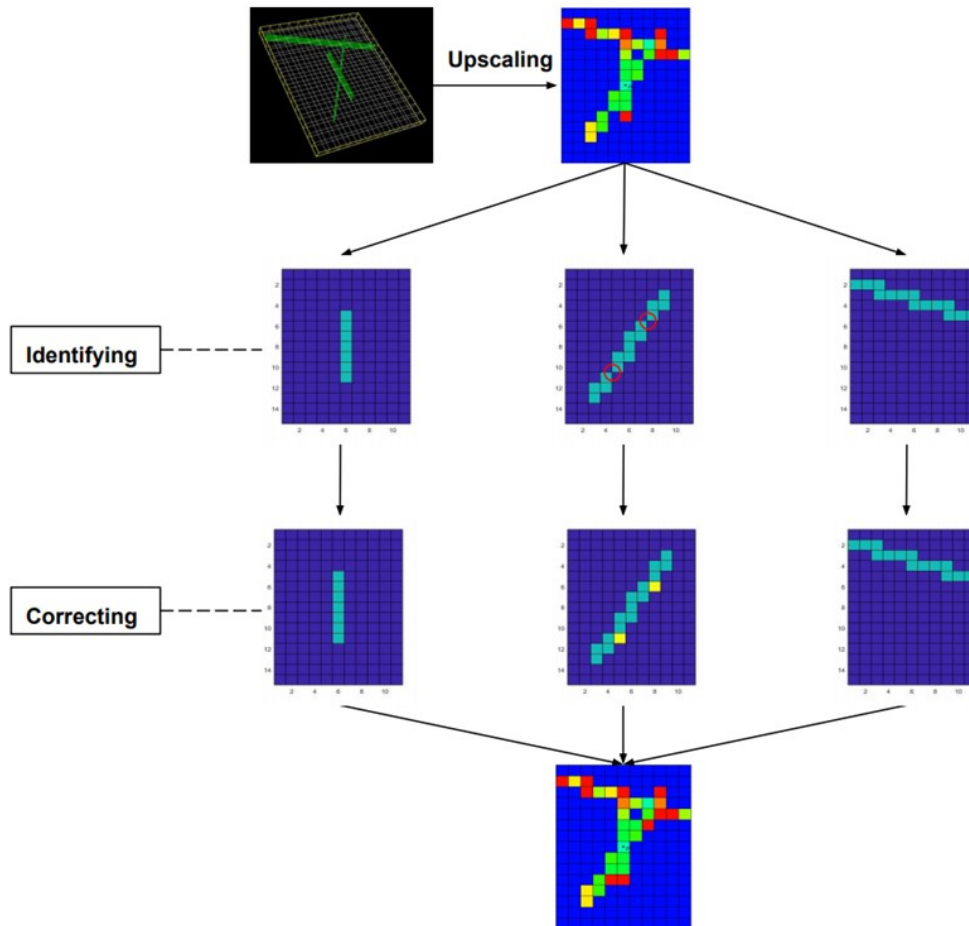
Fig. 3.3. Proposed workflow of the identification and correction processes.

3.3.1. Identifying Disconnections

First, for each fracture in the DFN, locations (i.e., coordinates) of a fracture plane are used to identify and label all grid blocks that should have been intersected. In 2D, this step can be facilitated by dividing each fracture line into many shorter sub-segments and marked by a series of points (i.e., endpoints of each sub-segment). The coordinates of these points are compared to the cell corners: a fracture line is intersecting a particular grid cell if at least one of these end-points is residing within that grid cell. Undoubtedly, dividing each fracture line into many sub-segments would lead to more accurate results, but it would also increase the overall computational efforts; therefore, a reasonable balance between accuracy and efficiency should be considered. Alternatively, the midpoints of each sub-segment can be used as well. A schematic of the two segmentation (point allocation) schemes is illustrated in Fig. 3.4. In 3D, the same idea applies, except that each fracture plane is divided into a series of 2D sub-planes; corners or centers of these sub-planes are examined, as shown in Fig. 3.5. The result of this step is a list of cells intersected (or should be connected) by a given fracture. There are as many lists as there are the number of fractures.
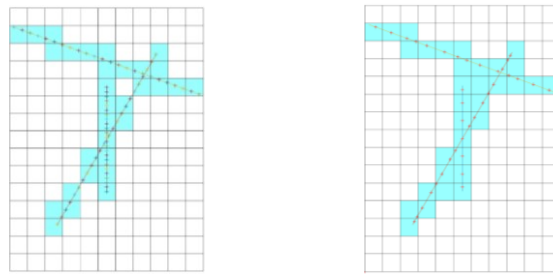
Fig. 3.4. Illustration of the two segmentation methods: end-points of each sub-segment are shown (left); mid-points of each sub-segment are shown (right).

Fig. 3.5. Segmentation scheme for 3D fracture planes.

Next, the connected cell lists (from previous step) are compared to the original DPDK model (with missing connections); for example, for fracture #1, if the connected cell list consists of 5 cells, the DPDK model is then examined to see if those 5 cells have non-zero fracture properties. Finally, blocks that should have been connected but having missing fracture properties are identified and labeled as "missing connections". This check is repeated until all fractures are checked. This process is illustrated in Fig. 3.6.
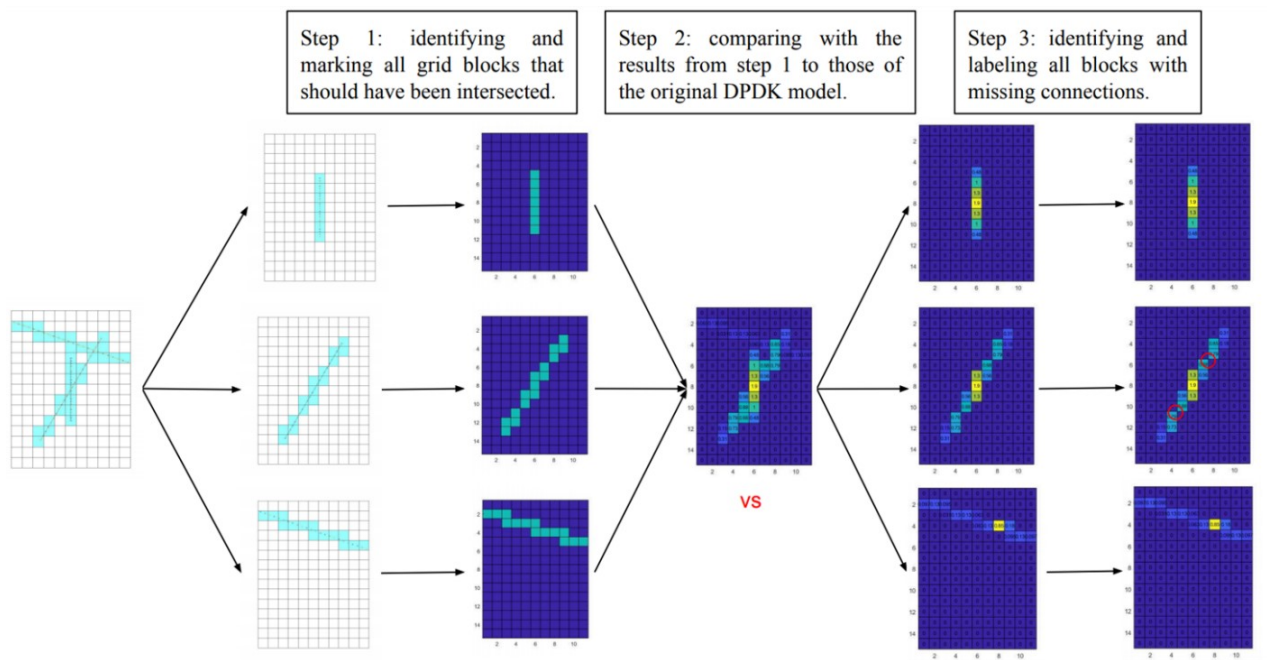
Fig. 3.6. Demonstration of identifying the missing connections. Fracture permeability is used as an example in the diagram.

Finally, gird blocks that are erroneously disconnected with missing fracture parameters are identified. The procedure described thus far is capable of detecting essentially all the erroneously disconnected cells. The only exception may be those where the two cells are connected at the corners. Fig. 3.7 illustrate two examples where the connected grid cells are missing. It is worth mentioning that the situation Fig. 3.7(b) may be hard to detect if there are not sufficient sub-segments, such as those shown in Fig. 3.4. An additional subroutine is added to identify this special case in 2D; a similar scheme is developed for 3D, as shown in Fig. 3.8, and a pseudocode is generated to illustrate the process shown in Fig. 3.9. The outcomes of this step are a list of all grid blocks that should be intersected by at least one fracture and which fracture(s) is(are) corresponding to a certain grid block.

(a)   (b)

(c)
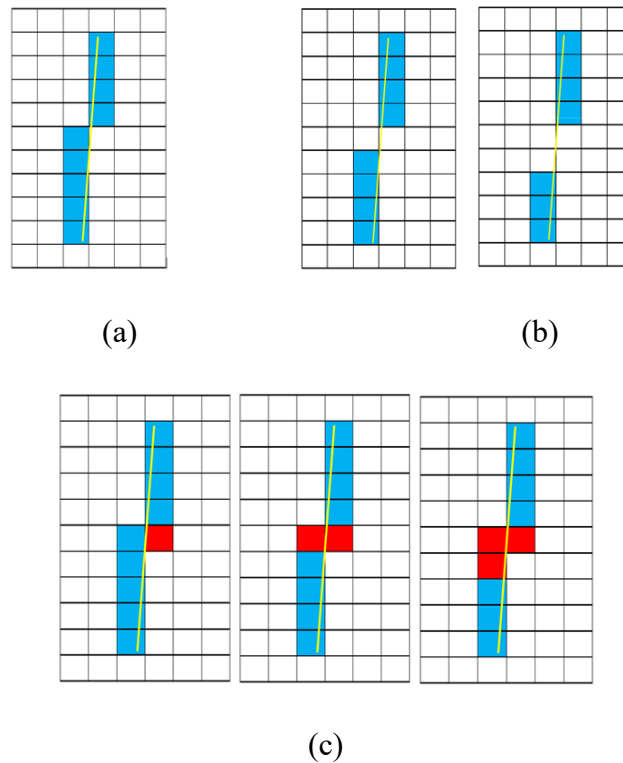
Fig. 3.7. (a-b) Examples of fractures being disconnected after upscaling in 2D. (c) A connection can be re-established by adding certain fracture parameters to the red cells. The yellow line represents the fracture; the blue grid blocks have upscaled fracture parameters after upscaling.

23

(a)Fracture blocks are
connected along one edge

(b)Fracture blocks are connected
at one corner
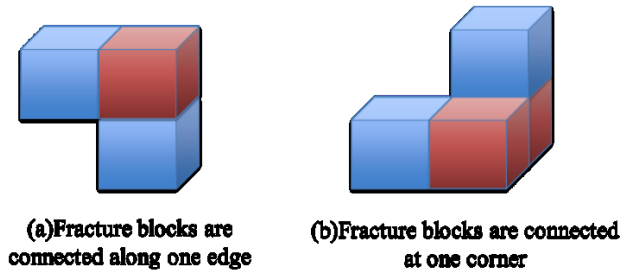
Fig. 3.8. Examples of fractures being disconnected after upscaling in 3D. A connection can be re-established by adding certain fracture parameters to the red cells. Blue grid blocks have upscaled fracture parameters after upscaling.

Initiate upscaled_value; // *upscaled value is equal to fracture spacing, fracture permeability or fracture porosity//*

Set all the values not equal to 0 equal **to** 1 in upscaled_value; // *using 0 to represent a gird block is empty and 1 to represent having value//*

Assign upscaled_value **to** upscaled_value_new;

Assign upscaled_value **to** upscaled_value_compare;

Assign 0 **to** stop_sign;

Loop as long as stop_sign~=1 is **True**

   For k from 1 to the mesh size in z direction

     For i from 1 to the mesh size in x direction

       For j from 1 to the mesh size in y direction

         If upscaled_value_new(i,j,k)==1

           If fracture blocks are connected along one edge

             Assign 1 **to** upscaled_value_new edge grid block;

           Elseif fracture blocks are connected along one corner

             Assign 1 **to** upscaled_value_new edge grid block;

             Assign 1 **to** upscaled_value_new corner grid block;

  If upscaled_value_new == upscaled_value_compare

    Assign 1 **to** stop_sign;

  Elseif upscaled_value_new ~= upscaled_value_compare

    Assign 0 **to** stop_sign;

  Assign upscaled_value_new **to** upscaled_value_compare;

If upscaled_value(i,j,k) ~= upscaled_value_new(i,j,k)

  Assign 3 **to** upscaled_value(i,j,k); // *Using 3 to represent the missing grid block//*

Fig. 3.9. Pseudocode for identifying the disconnected grid blocks in 3D.

24

3.3.2 Correcting Disconnections

To re-established a connection between these disconnected fracture blocks, fracture parameters should be added to those missing connected cells, as denoted as red blocks in Figs. 3.7-3.8. Two formulations or options are proposed below, the workflow is shown in Fig. 3.10, and a pseudocode is presented in Fig. 3.11:

1. Identify a group of nearby cells and re-distribute the fracture parameters over these cells.

2. According to the "sugar cube" model, the maximum values of fracture spacing would correspond to the grid block dimensions (Δx, Δy, and Δz). Therefore, the fracture spacing in the missing connected block can be assigned as equal to the grid block dimensions. The advantage is that the fracture spacing of the neighboring grid blocks remains unaffected. Fracture permeability and fracture porosity are modified in the same fashion as the previous option.
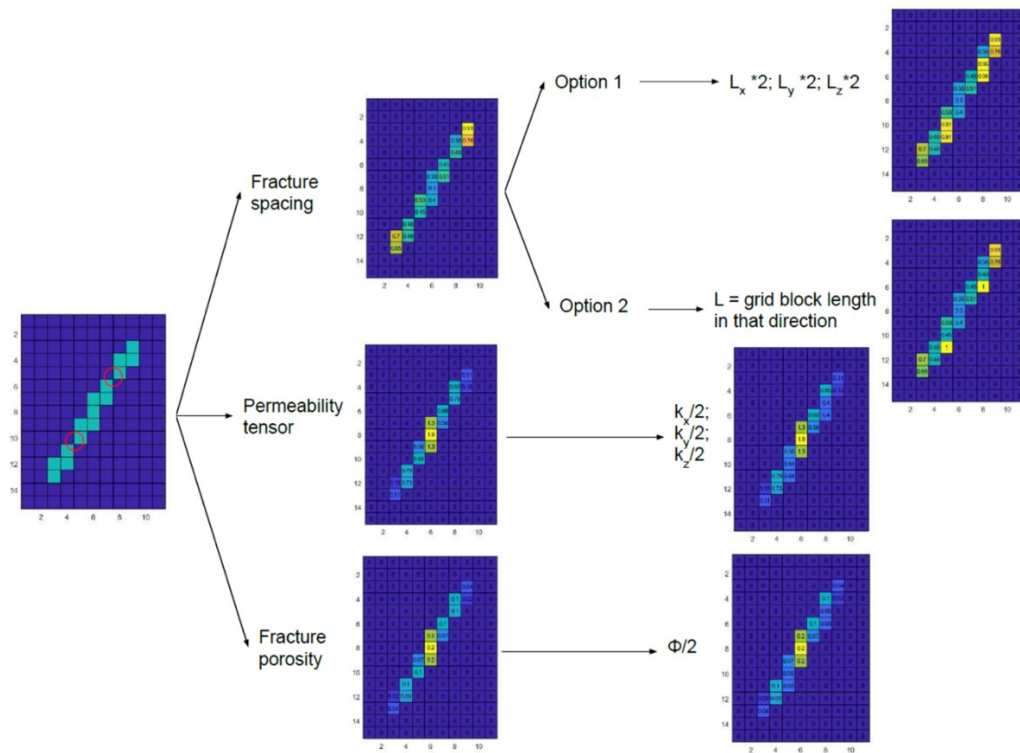
Fig. 3.10. Two formulations for correcting disconnected grid blocks.

```
Initiate upscaled_value; // Value is equal to fracture spacing, fracture permeability or fracture porosity//
Set all the empty values in the upscaled_value equal to 0;
For k is from 1 to the mesh size in z direction
    For i is from 1 to the mesh size in x direction
        For j is from 1 to the mesh size in y direction
            If upscaled _value is fracture permeability or fracture porosity
                If upscaled_value(i,j,k) is identified to be missing
                    Assign upscaled_value in the nearby grid block/2 to upscaled_value(i,j,k);
            Elseif upscaled_value is fracture spacing
                If upscaled_value(i,j,k) is identified to be missing
                    Option 1: Assign upscaled_value in the nearby grid block*2 to upscaled_value(i,j,k);
                    Option 2: Assign grid block length to upscaled_value(i,j,k);
```

Fig. 3.11. Pseudocode for correcting the disconnected grid blocks.

This correction step is carried for each fracture sequentially. In the end, all the pre-existing and updated fracture parameters must be assembled. During this step, it is important to check if the newly-connected grid block is intersected by more than two fractures, as shown in Fig. 3.12. In that case, the final permeability and porosity of that cell would be the sum of contributions of both fractures (i.e., via simple addition, according to Eqs. (3.9)-(3.10), while for the fracture spacing, option 2 is used, where the grid block size is assigned.
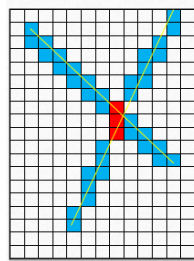
Fig. 3.12. Illustration of two intersecting fractures.

Chapter 4: Tight Oil Production Simulation

This chapter presents a set of 2D and 3D tight oil models in a black-oil system based on typical properties gathered from the Bakken formation. The results for both the original DPDK model and corrected DPDK model are compared and two correcting options are discussed. Also, the equivalent EDFM simulations are constructed to assess the improvement of the corrected model. It also presents a sensitivity analysis evaluating the impacts of mesh resolution and DFN properties on the upscaling performance.

4.1 Case Study I: 2D Example

The method is tested first using a 2D tight oil simulation model. One stage of hydraulic fracturing for a horizontal well in the Middle Bakken formation is simulated. Most of the model parameters are extracted from a previous study based on field data (Yue et al., 2016). In addition to the hydraulic fracture, a DFN is incorporated to model a network of secondary fractures. The hydraulic (primary) fracture is modeled explicitly, with local grid refinement (LGR) being implemented in the nearby region around the primary fracture. The DFN is subsequently upscaled to an equivalent DPDK. The model set-up is shown in Fig. 4.1. The relevant model parameters are summarized in Table 1. Several references have reported the in-situ stress being $\sigma_v \geq \sigma_H > \sigma_h$, and faults are primarily vertical or sub-vertical normal ones; therefore, the natural (secondary) fractures are assumed to have a plunge angle of 0 degrees (Wang, 2011).
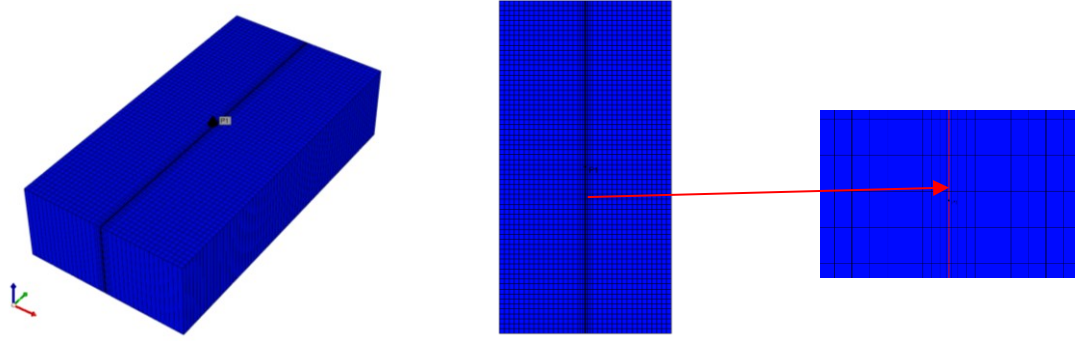
Fig. 4.1.Model set-up for the 2D example (only one grid cell is in the vertical z-direction).

Table. 4.1. Reservoir and fracture properties.

Reservoir		Unit	Initial Conditions		Unit
Dimension	136×264×5	m	Reservoir pressure	46884	kPa
Matrix permeability	0.0005	mD	Reservoir temperature	338	K
Matrix porosity	0.09		Oil-water contact depth	3000	m
Rock compressibility	2.51E-06	1/kPa	Bubble point pressure	35000	kPa
Oil compressibility (over 35 MPa)	4.40E-06	1/kPa			
Oil viscosity (over 35 MPa)	0.56	cP			

Hydraulic Fracture		Unit	Secondary Fracture		Unit
Half-length	132	m	Trend angle	$X \sim N(30, 20)$	degree
Width	0.01	m	Fracture intrinsic permeability	$X \sim N(10000, 1000)$	mD
Spacing	136	m	Fracture aperture	$X \sim N(0.001, 0.0001)$	m
Equivalent fracture permeability	256	mD	Fracture length	$X \sim N(70, 30)$	m
Intrinsic permeability	100000	mD	Number of fractures	20	

4.1.1 Correction of the Disconnected Grid Blocks

Twenty secondary fractures are modeled, as shown in Fig. 4.2 (a). The original upscaled fracture spacing values are shown in Fig. 4.2 (b). A detailed examination would reveal that the fractures are disconnected erroneously at 18 locations; they are detected via the described procedure and shown in Fig. 4.2(c).

Both correction options are implemented. The production profiles for the final (corrected) DPDK models are compared in Fig. 4.3. The base case refers to the original DPDK model (without

corrections). Similar results are obtained for both options, and the production has increased dramatically (~22%) when compared to the base case after 4.5 years. The impacts of the missing connections are further illustrated in Fig. 4.4, which shows the pressure distribution in the fracture cells after the first time step. The red circles indicate areas where the fractures have been erroneously disconnected in the original DPDK model. Re-establishing the connection has helped to increase fluid flow, as evidenced by an increase in pressure drop.

To further compare the two options, another set of DFN models (Fig. 4.5(b)), with different fracture permeability (100000mD, 10× the previous case), is constructed. The results are presented in Fig. 4.6, and, once again, no significant difference is observed between the two options. The following conclusion can be drawn from this case study: the production profiles are not strongly affected by the specific values assigned to the re-connected blocks; it is the restoration of the adjacent connectivity that has a significant impact on the overall conductivity within the fracture network.

(a)   (b)   (c)
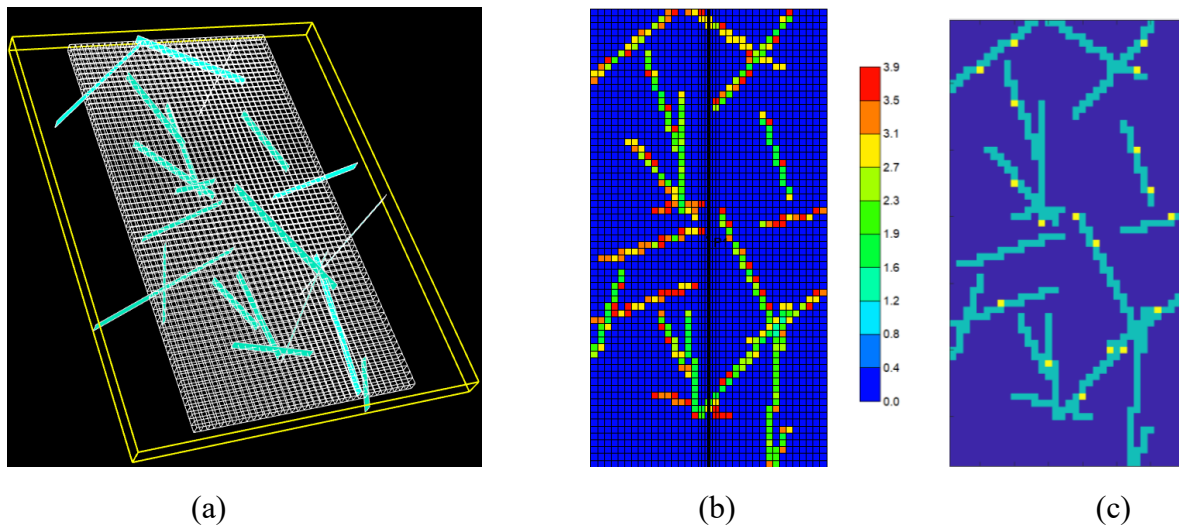
Fig. 4.2. (a) DFN model #1. (b) Upscaled fracture spacing in DPDK model. (c) 18 grid blocks, as denoted in yellow, indicate locations where connections are missing.

(a)

(b)
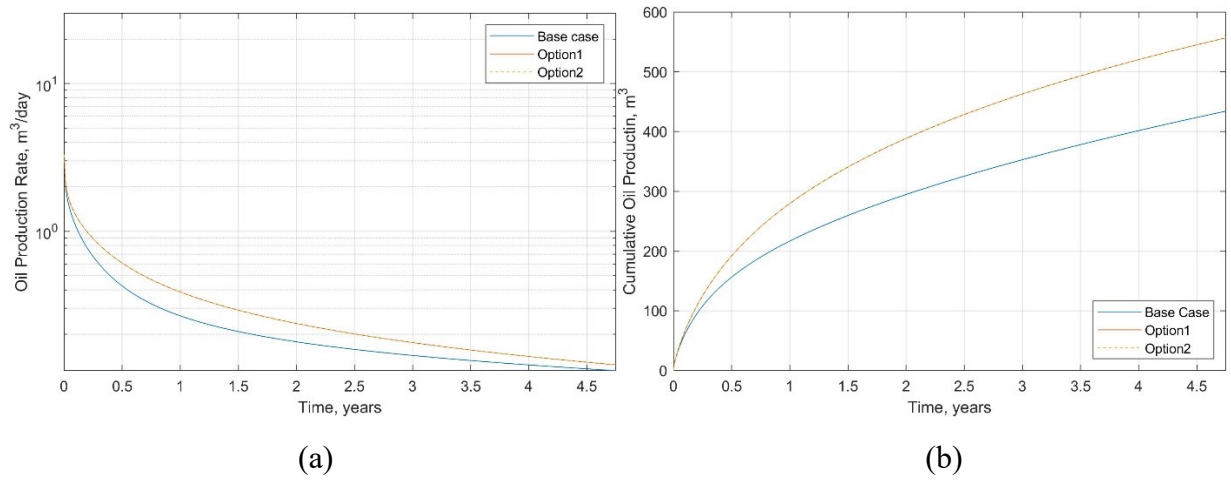
Fig. 4.3. Comparison of the base case and the two corrected models: (a) oil production rate; (b) cumulative oil production.

(a)

(b)
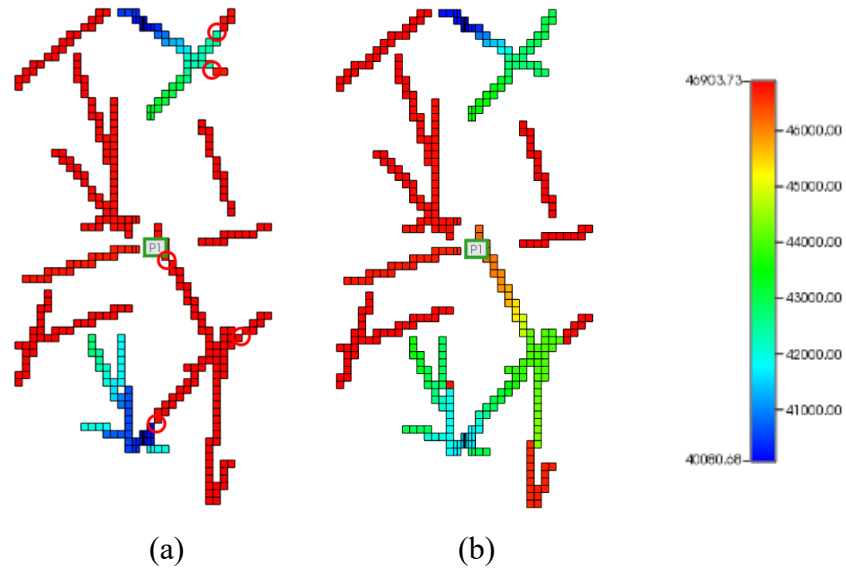
Fig. 4.4. Pressure distribution in the fracture grid cells after the first time step: (a) original DPDK model – no corrections making corrections; (b) corrected models. Regions with re-established connections are marked with red circles.

30

<div align="center">(a)   (b)   (c)</div>
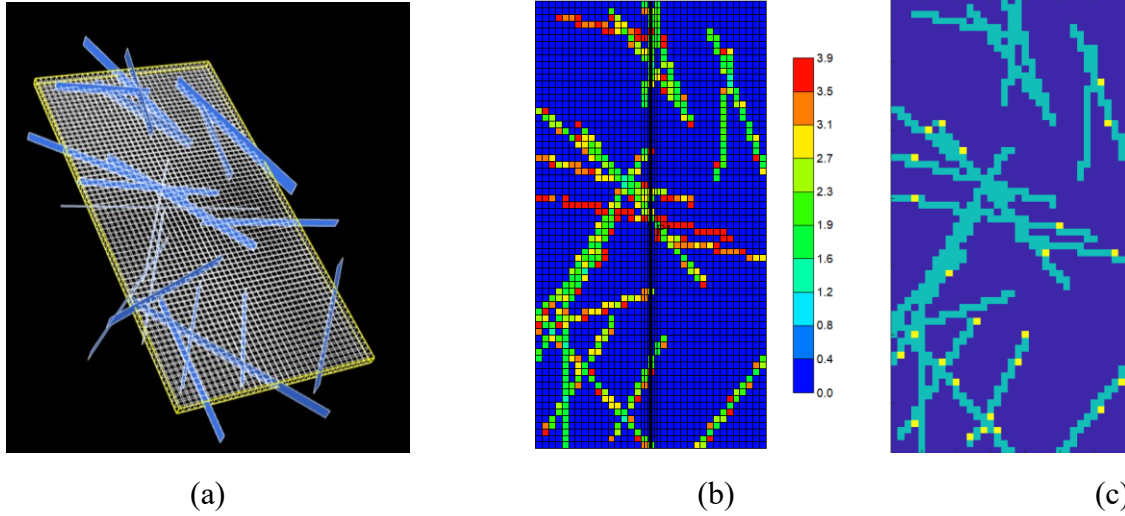
Fig. 4.5. (a) DFN model #2. (b) Upscaled fracture spacing in DPDK model. (c) 25 grid blocks, as denoted in yellow, indicate locations where connections are missing.

<div align="center">(a)   (b)</div>
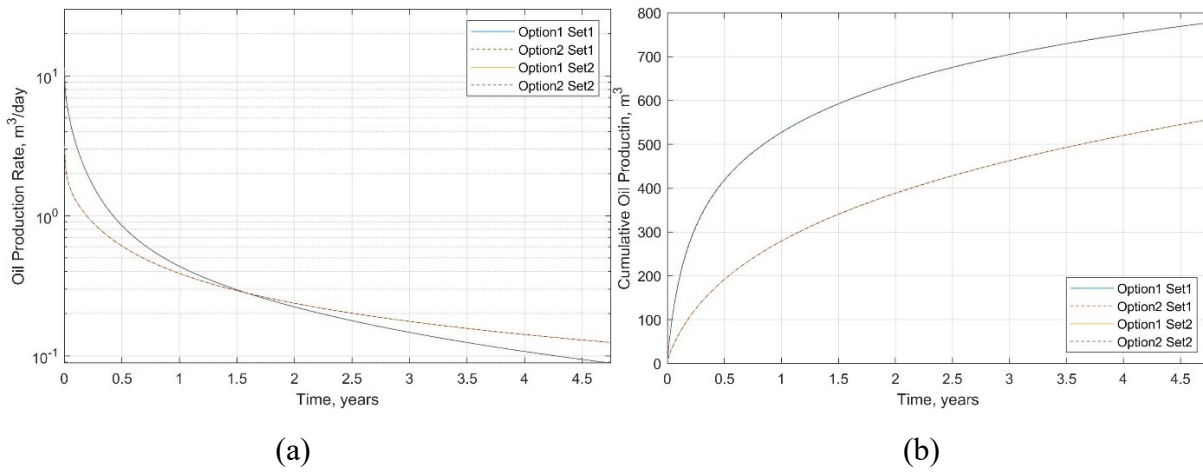
Fig. 4.6. Results of the DFN models: (a) oil production rate; (b) cumulative oil production.

4.1.2 Comparison with EDFM Model

In an EDFM framework, fractures are modeled explicitly and embedded within a grid block; the fracture-fracture and fracture-matrix connections are accounted for in the flow calculations. Fig. 4.7 (a) shows the grid system with a set of discrete fractures, and Fig. 4.7 (b) shows the non-neighboring connections (NNC) between fracture grids and matrix grids. In the context of this paper, it is assumed that the solution from EDFM is the accurate or true response. Therefore, the

objective here is to determine whether the corrected DPDK model would yield results similar to the EDFM response.

The EDFM flow simulation is implemented within the MATLAB Reservoir Simulation Toolbox (MRST) framework. MRST is an open-source reservoir simulation package (Lie, 2019). A couple of comparison models are constructed. First, a homogeneous model with no fractures is constructed based on parameters in Table. 4.1., and only one producer is located at the center. The simulated oil production profiles for the EDFM and corrected DPDK models are compared in Fig. 4.8, and the two responses are essentially identical. Next, a primary fracture (representing a hydraulic fracture) is added. In addition to the EDFM simulation, a single-porosity model is constructed where the fracture is discretized explicitly with local grid refinement (LGR). Among these three set-ups, it would be assumed that the single-porosity LGR case being the most accurate. The results are compared in Fig. 4.9, and it is interesting to note that the corrected DPDK results would more closely resemble the single-porosity LGR case. Finally, for the final case, both secondary fractures and a primary fracture are incorporated. The results for the EDFM and DPDK models (both original and corrected) are compared in Fig. 4.10. The corrected DPDK model can dramatically increase the accuracy of the simulation results when compared against the more sophisticated modeling approaches such as EDFM and single-porosity model with discrete fractures. The original DPDK with missing connections can underestimate the production by approximately 21.89%. It is also concluded either options (1 or 2) are effective.
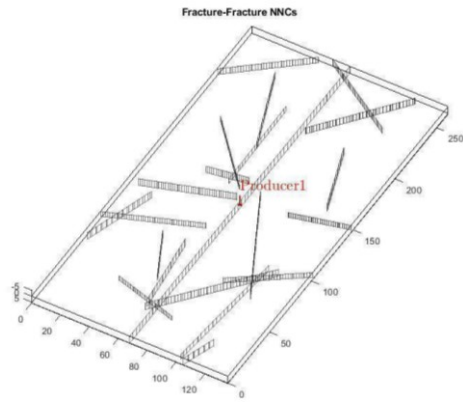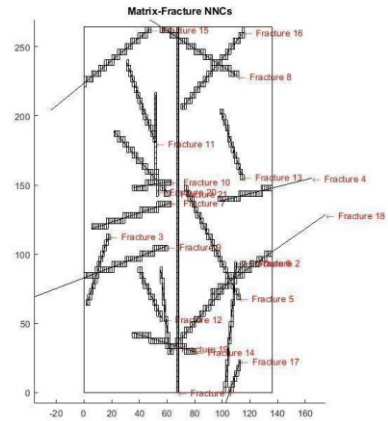
(a)   (b)

Fig. 4.7. (a) EDFM mesh. (a) Non-neighbouring connection between fractures and matrix.
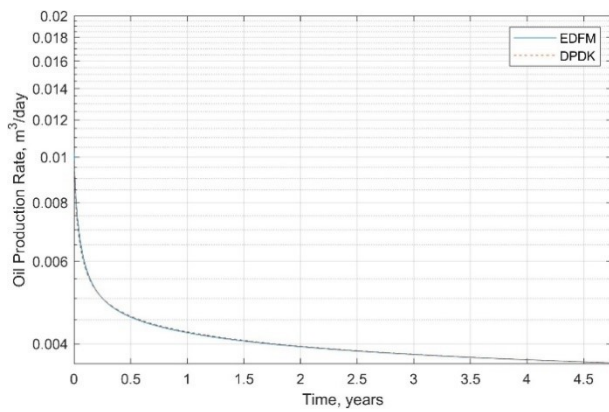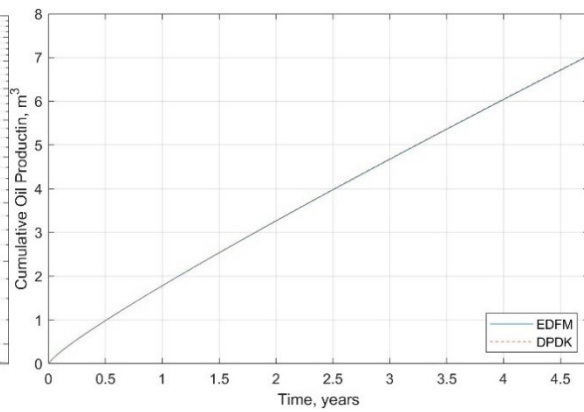
(a)   (b)

Fig. 4.8. Comparison of EDFM and corrected DPDK models for simulating a homogeneous domain: (a) Oil production rate; (b) Cumulative oil production.

33

(a)   (b)
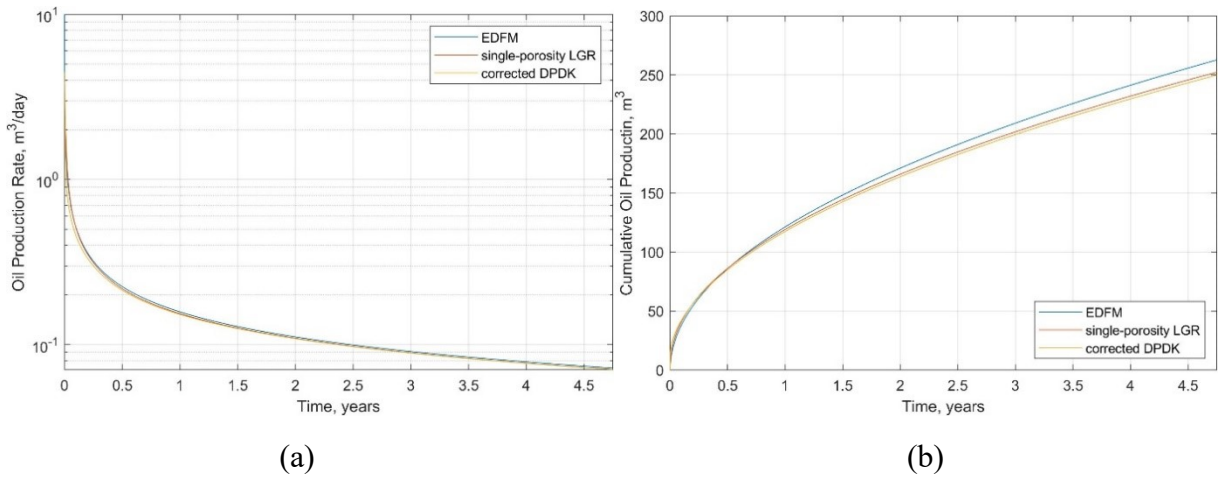
Fig. 4.9. Comparison of EDFM, single-porosity LGR, and corrected DPDK models for simulating a single-stage of hydraulic fracturing: (a) Oil production rate; (b) Cumulative oil production.

(a)   (b)
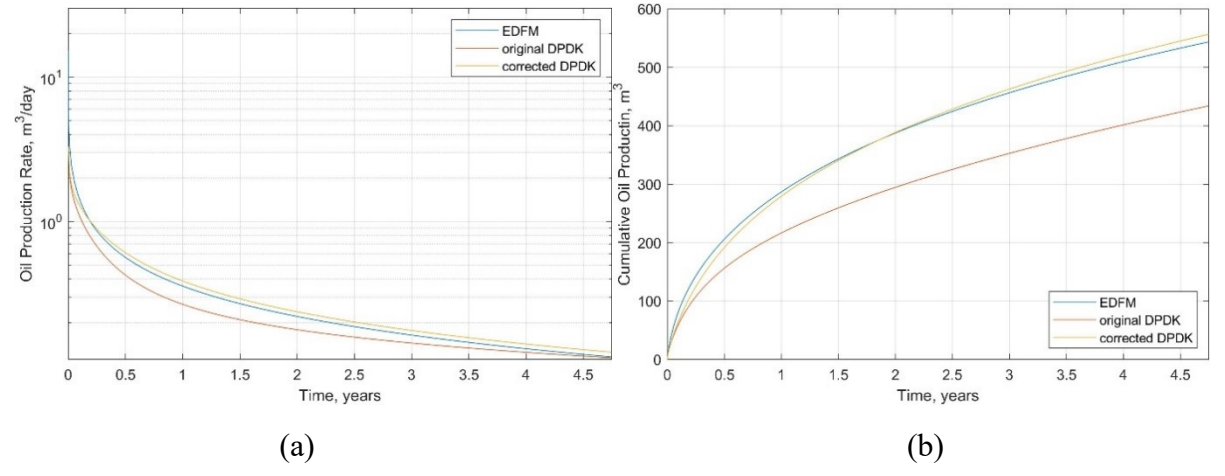
Fig. 4.10. Comparison of EDFM, original and corrected DPDK models: (a) Oil production rate; (b) Cumulative oil production.

4.2 Case Study II: 3D Example

A 3D model is constructed based on the same Bakken reservoir parameters. A reservoir thickness of 150 ft is assumed (Wang, 2011). The DFN model is shown in Fig. 4.11(a); 100 natural fractures are modeled. After upscaling, a total of 529 disconnected grid blocks are detected (these are cells

where fracture parameters are missing in the DPDK model). Connections are re-established based on the method described.

Fig. 4.12 is showing the pressure distribution after one-month of production for layer 5. It is observed the corrected DPDK model predicts a larger pressure drop. The result for oil production rate and cumulative oil production profiles are shown in Fig. 4.13 (a) and (b). The cumulative oil production significantly increases for the corrected DPDK model (i.e., the production is underestimated by approximately 10% if the fracture grid blocks are erroneously disconnected). The corrected model helps to re-establish the overall conductivity of the entire fractured system.

The negative effect of disconnected blocks is less severe in 3D than in 2D. This is because it is less likely to completely partition a fracture plane in 3D into multiple disconnected portions after upscaling. However, this phenomenon is more probable when a fracture plane in 2D (i.e., a line) is upscaled.

(a)   (b)
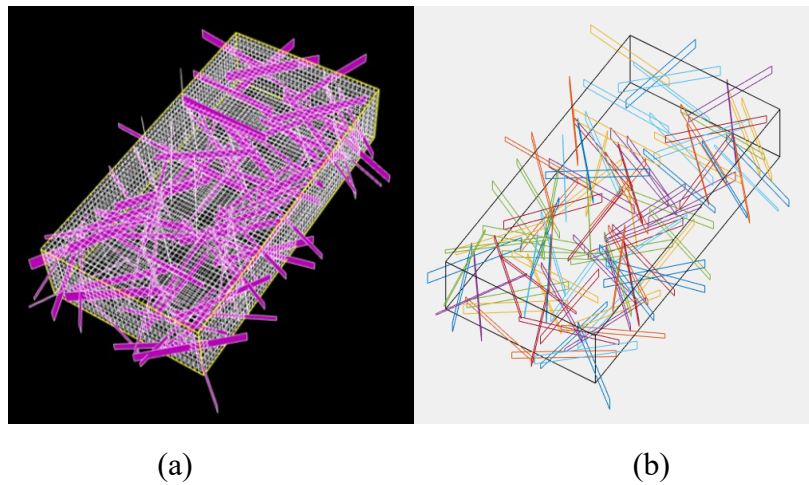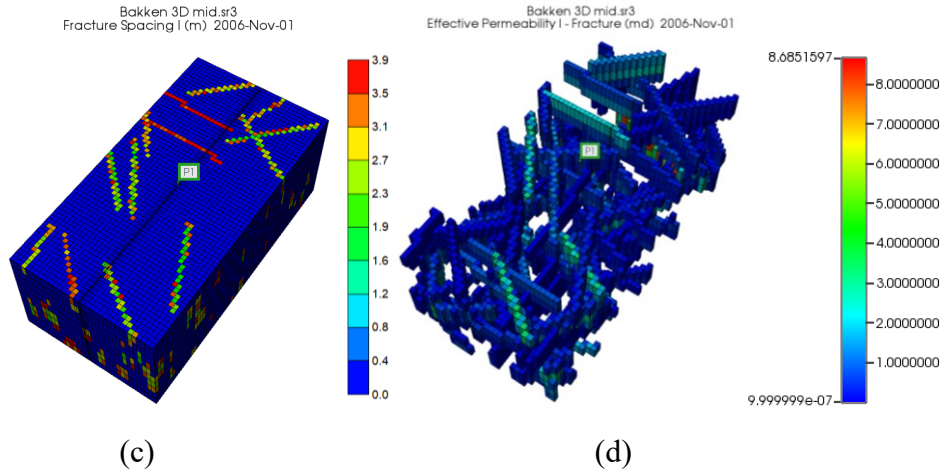
Fig. 4.11. 3D model – (a) DFN model; (b) extracted fracture network; (c) fracture spacing in I direction in the corrected DPDK model; (d) diagonal element of effective fracture permeability tensor in the I direction in the corrected DPDK model.
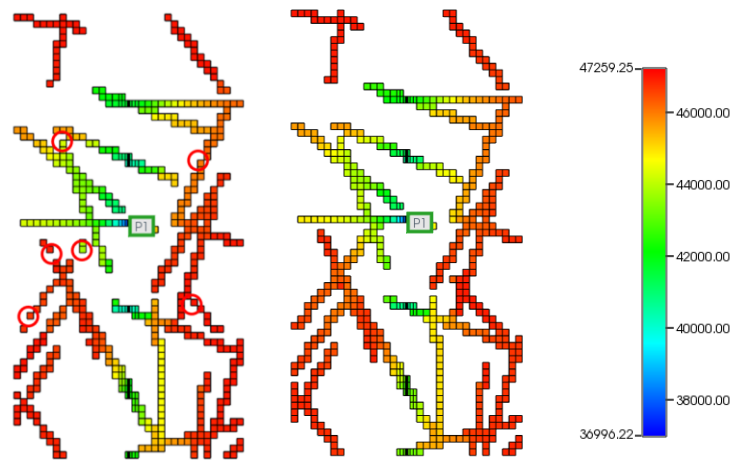
Fig. 4.12. Pressure distribution in layer 5 after a one-month of production for the original (left) and corrected (right) DPDK models.
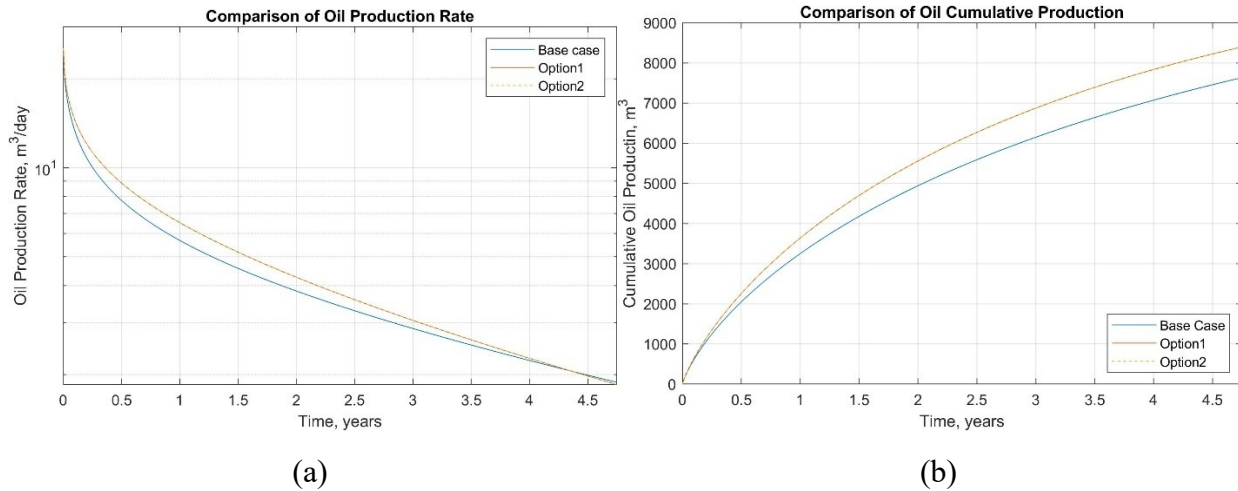
Fig. 4.13. Comparison of the original and the two corrected DPDK models (options 1 and 2) – (a) Oil production rate; (b) Cumulative oil production.

4.3 Sensitivity Analysis

A sensitivity analysis is conducted to assess the impacts of mesh resolution and certain DFN parameters on the upscaling performance. Multiple DFN models are generated and upscaled into different DPDK models with varying mesh resolution (i.e., grid sizes). The objective is to assess how are connections between fractures retained or removed for different mesh sizes and fracture properties (e.g., fracture density, fracture length, and fracture angle).

4.3.1 Grid Meshing

The domain size is 100 m × 200 m × 20 m, and the fracture parameters are the same as those presented in Table. 1. A DFN model consisting of ten fractures and an average fracture length of 70 m is constructed. The model is upscaled to five DPDK meshes of different sizes. The results are summarized in Table. 4.2. The result shows the number of missing grid blocks increases almost linearly as the total number of grid blocks increases, and the proportion of missing grid block in relation to the total number of fracture grid blocks in the final corrected model increases from 1.7

37

% to 4.2 % as the mesh becomes more refined. And from Table 4.2(b) we can observe, because of the increase of the missing connection, as the mesh is getting finer, the error increases from 6.2% to 28.06%.

The cumulative oil production profiles are shown in Fig. 4.14. The results are less sensitive to the mesh size for the corrected model. Without re-establishing the missing connections, the model may underestimate the oil production by 6 to 28%. The results reveal that DPDK upscaling is more sensitive to grid refinement.

After correction, the relationship between the corrected DPDK model is compared with the equivalent EDFM model. As shown in Fig. 4.15, the result of cumulative oil production from the EDFM model is below those of the DPDK models. Also, as the DPDK mesh is finer, the cumulative production profile is closer to that of EDFM. The result is consistent with the statement of Hui et al. (2019) about the DPDK model what illustrates the equivalent model like DPDK can over-connect the fractures.

Table. 4.2(a). Number of missing (disconnected) grid blocks for different 2D mesh sizes.

Dimension	Meshing scheme (number of grid blocks in each direction)	Total grid blocks	Number of missing (disconnected) grid blocks (A)	Number of fracture grid blocks in the original DPDK model (B)	Percentage of missing blocks (A/B)
100×200×20	41×81×1	3321	6	343	1.75
100×200×20	51×101×1	5151	9	430	2.09
100×200×20	61×121×1	7381	19	511	3.72
100×200×20	71×141×1	10011	23	599	3.84
100×200×20	81×161×11	13041	29	686	4.23

Table. 4.2(b). Cumulative oil production for different 2D mesh sizes.

Meshing scheme (number of grid blocks	Cumulative oil production of original DPDK model (m^3) (A)	Cumulative oil production of the corrected DPDK model (m^3) (B)	Difference (m^3) (A-B)	Error = difference/B (%)

in each direction)				
41×81×1	1291.65	1377.09	85.44	6.20
51×101×1	1140.19	1357.84	217.65	16.03
61×121×1	1107.07	1348.53	241.46	17.91
71×141×1	1004.51	1327.63	323.12	24.34
81×161×11	951.20	1322.18	370.98	28.06
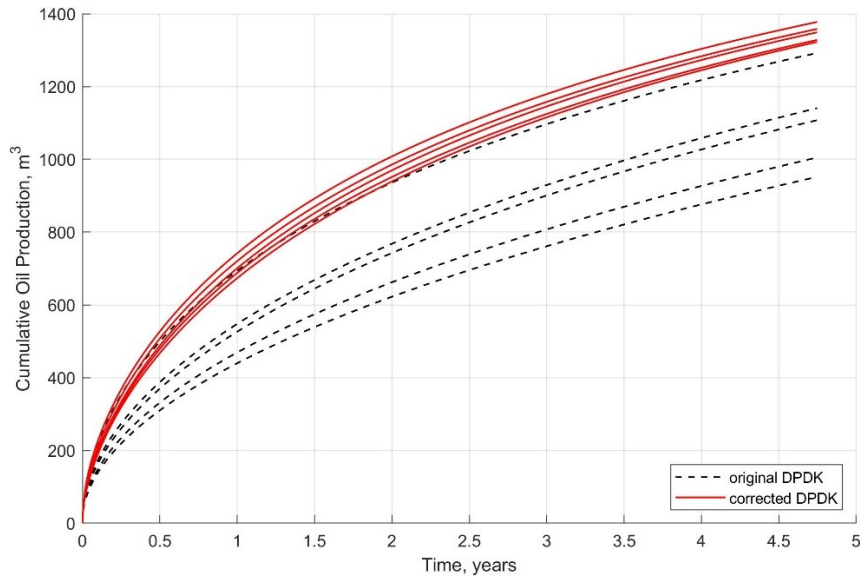
Fig. 4.14. Cumulative oil production profiles for the corrected DPDK model using different mesh sizes.
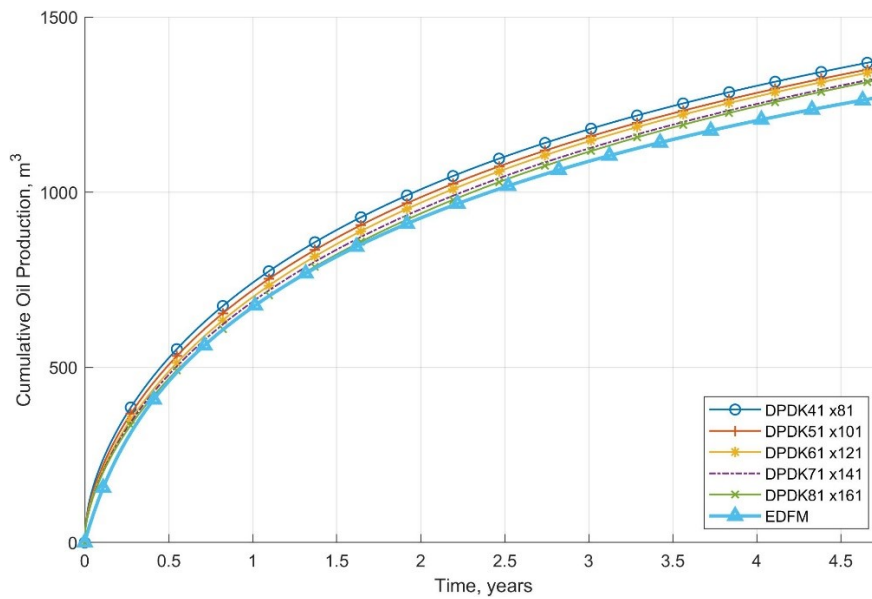
Fig. 4.15. Comparison of cumulative oil production between the DPDK model with different meshing and the EDFM model.

4.3.2 Fracture Density and Fracture Length

The domain size is 100 m × 200 m × 20 m with a meshing of 20 ×40 × 10. Twenty-four DFNs corresponding to six different fracture densities and four different fracture lengths are constructed to study their effects on upscaling performance.

The results are summarized in Table. 4.3 and shown in Fig. 4.15. As expected, as fracture density (defined as the total number of fractures in the model) increases, the number of missing fracture blocks also increases, regardless of the fracture length. However, as the fracture density is increased beyond a certain threshold (~ 500 – 1000 fractures), the number of missing fracture blocks gradually decreases until it reaches zero (as fractures are present in all grid blocks).

The effect of fracture length is quite interesting: at low fracture density, the increase of fracture length will lead to an increase in the number of missing fracture blocks; conversely, at high fracture density, an increase in fracture length leads to a decrease in the missing fracture blocks. This is because, for a fixed number of fractures, there are likely more disconnected blocks if the fractures are longer. However, when there are too many fractures, longer fractures would mean that almost all grid blocks are intersected by at least one fracture, so the number of missing fracture blocks is reduced.

Table. 4.3. The change of missing grid blocks with an increase of DFN length and fracture density.

Fracture length (m)	Fracture density (#)	Number of disconnected fracture blocks	Number of total fracture cells in the final corrected DPDK model
10	10	30	82
	50	105	281
	100	192	463
	500	682	2089
	1000	1033	3706
	5000	251	7629
30	10	48	120
	50	167	601
	100	350	1320
	500	796	4046
	1000	649	6271

	5000	12	7984
50	10	67	177
	50	215	837
	100	405	1720
	500	634	5693
	1000	364	7103
	5000	1	7999
70	10	79	326
	50	237	1066
	100	453	2134
	500	533	6016
	1000	200	7592
	5000	0	8000
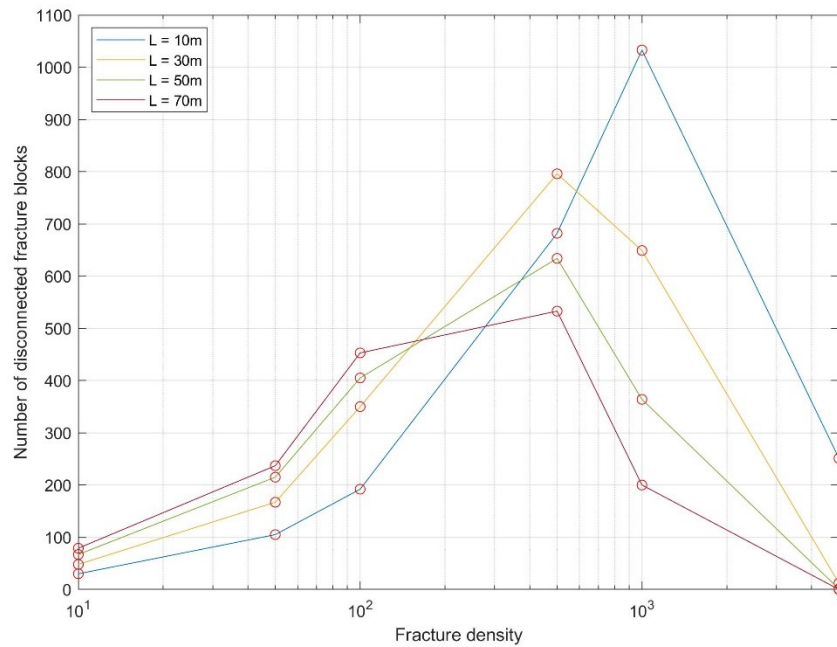
Fig. 4.16. The number of missing fracture blocks as a function of fracture density and length (*L*).

4.3.3 Fracture Orientation

In many cases, fractures are not aligned with the coordinate axes, and their impacts are examined here. Five different trend angles (5, 15, 25, 35, and 45 degrees) are upscaled to a DPDK model of 100 m × 200 m × 20 m and a mesh of 20 × 40 × 1. The results in Fig. 4.16 show that an increase

in trend angle would lead to more misalignment and the number of missing fracture blocks would

increase.
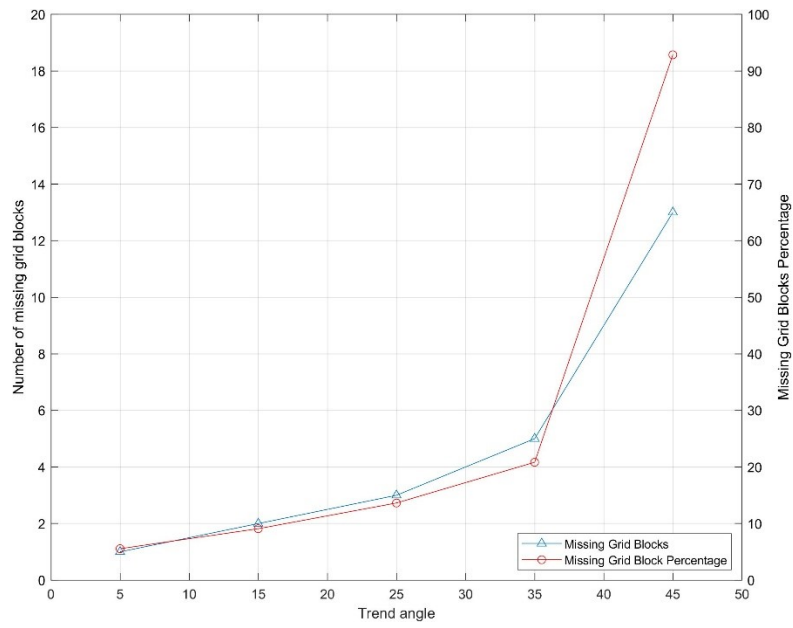
Fig. 4.17. The number of missing fracture blocks as a function of trend angle.

Chapter 5: Simulation of Hydraulically Fractured Well Performance During Flowback

5.1 Introduction

After fracturing, the well is typically shut in to allow fracturing fluid to flow into the formation before the production, which is often referred to as the soaking period (Fan et al., 2010). While some field cases may suggest that prolonged soaking could negatively affect post-flowback production (Shaoul et al. 2011; Yan et al. 2015), other studies have shown that soaking could be beneficial to production and leads to higher long-term cumulative production (Fakcharoenphol et al., 2013; Yaich et al., 2015). Mineralogy could play a role, as it affects the interaction of fracturing fluids and the rock formation (Shaibu, 2020). Research has shown that the soaking period would lead to a redistribution of the injected fracturing fluid and in-situ reservoir fluids.

After soaking period, flowback is followed to discharge the fracturing fluid and debris remaining in the well. Flowback is essential and usually designed within the critical drawdown pressure limit to avoid the possibility of losing the integrity of the pumped proppant (Acock, 2004).

Therefore, simulating the fluid distribution during the soaking period and subsequent flowback performance is of great interest. Recently, the numerical simulation method has been implemented in a large number of studies to understand the mechanisms of the flowback process (e.g., Cheng, 2012; Wang, 2016; Li at el, 2017; Li et al, 2019). In this chapter, we will apply our proposed technique to construct a series of properly connected DPDK models to examine the effects of fracture connectivity on fluid distribution during the soaking period and production performance during flowback.

5.2 DPDK Flow Simulation

5.2.1 Model Set-Up and Initialization

A 2D DPDK model is set up to simulate the soaking, flowback, and production by using the same reservoir and fracture information in Table. 4.1. The model set-up follows the same strategies as presented in Liu et al. (2019) and Zhong & Leung (2020): It is assumed that the in-situ (initial) condition immediately after the completion of hydraulic fracturing can be modeled by assigning the initial pressure in the fracture to be the minimum stress, such that the fracture would stay open. The leak-off volume, which is usually modelled by an injection phase is ignored in this simplified approach because (1) the leak-off coefficient in shale/tight reservoir is normally extremely low (on the order of 0.00001 ft/min$^{0.5}$) (Shiozawa and McClure, 2016; Wu and Olson, 2016), and (2) the fracture-propagation phase is very short (less than a few hours). Also, the fracture is assumed to be uniformly propped, fully opened, and filled with fracturing fluid; therefore, the initial water saturation in both the main (primary) hydraulic fracture, as well as any connected secondary fractures, is assumed to equal to one. The parameters used for the model set-up are shown in Table. 5.1, and Fig. 5.1compares the initial water saturation distribution for the base case before and after correction. It is clear in Fig. 5.1(b) that re-establishing the connections leads to more water being distributed throughout the system initially (i.e., right after the completion of hydraulic fracturing, just before the soaking period).

Table. 5.1. Parameters for the model set-up.

Parameters	Values	Unit
Shut-in time	30	Day
Initial water saturation in the fracture	1	
Initial pressure in the fracture	50000	kPa
Well pressure	35000	kPa

<div align="center">(a)   (b)</div>
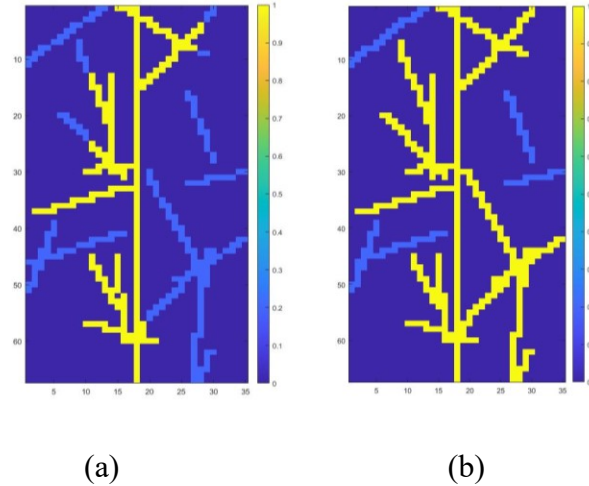
Fig. 5.1. Initial condition of water saturation. (a) Before correction; (b) after correction.

5.2.2 Results and Discussion

From Fig. 5.1(a), erroneously removed upscaled parameters at certain grid blocks would affect the connection between natural fractures and the main fractures. After performing the correcting method, the initial water saturation is presented in Fig. 5.1(b), which shows all the fractures filled with a fracturing slurry are correctly identified. There are significant differences in the production profiles for the original and corrected DPDK models. First, there is a very significant increase in oil production rate and cumulative oil, as shown in Fig. 5.2 for the corrected model; second, the well begins producing oil slightly sooner upon reopening. In Fig. 5.3, the pressure distribution after a 4.75-year production is presented; more oil production also results in a larger pressure decline for the corrected DPDK model. Besides, Fig. 5.2(c) reveals the corrected DPDK model has a higher water production rate during the first two years, resulting in an increase of cumulative water production shown in Fig. 5.2(d).
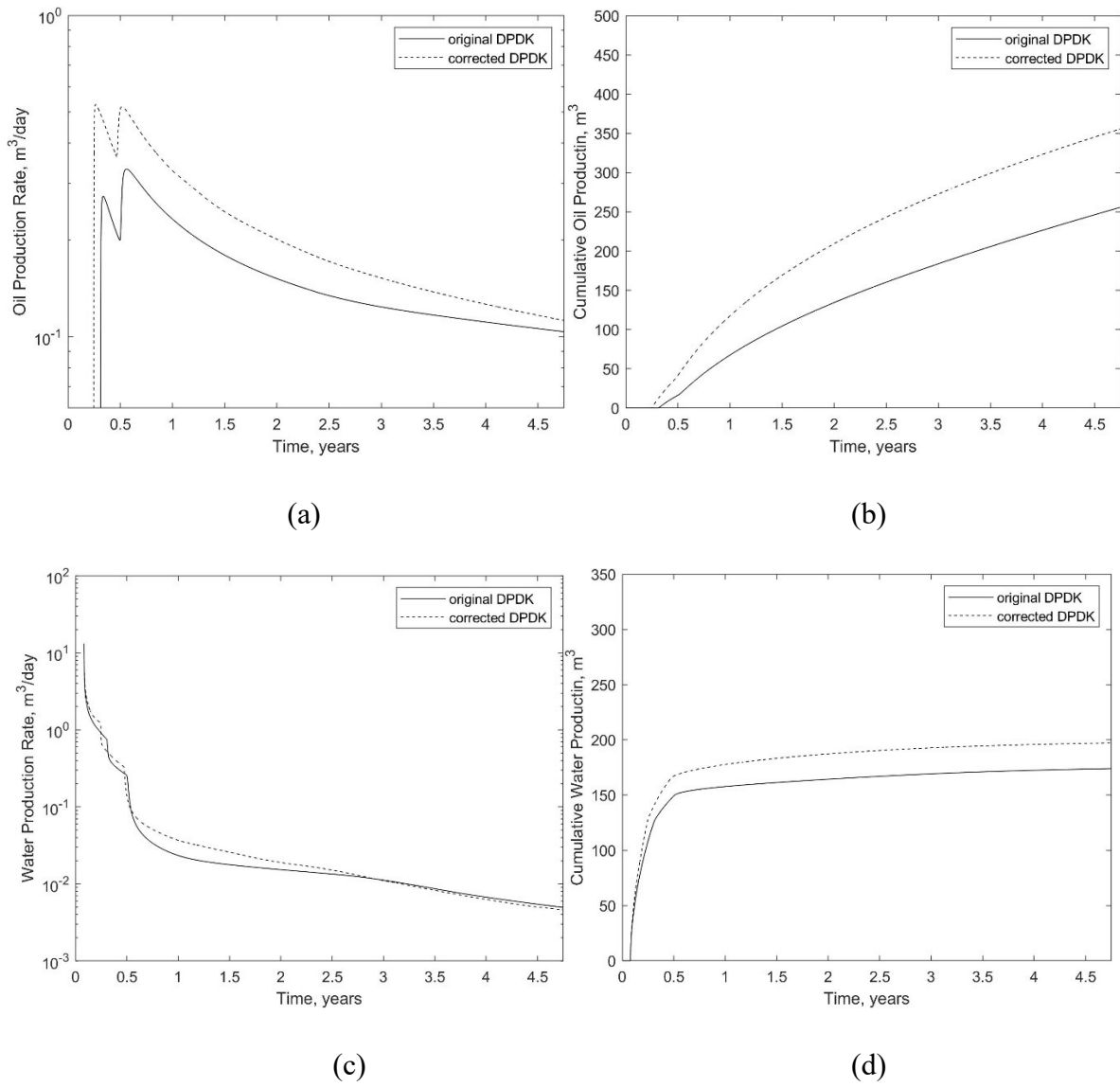
Fig. 5.2. Comparison of the cases before and after correction. (a) Oil production rate; (b) cumulative oil production; (c) water production rate; (d) cumulative water production.

46
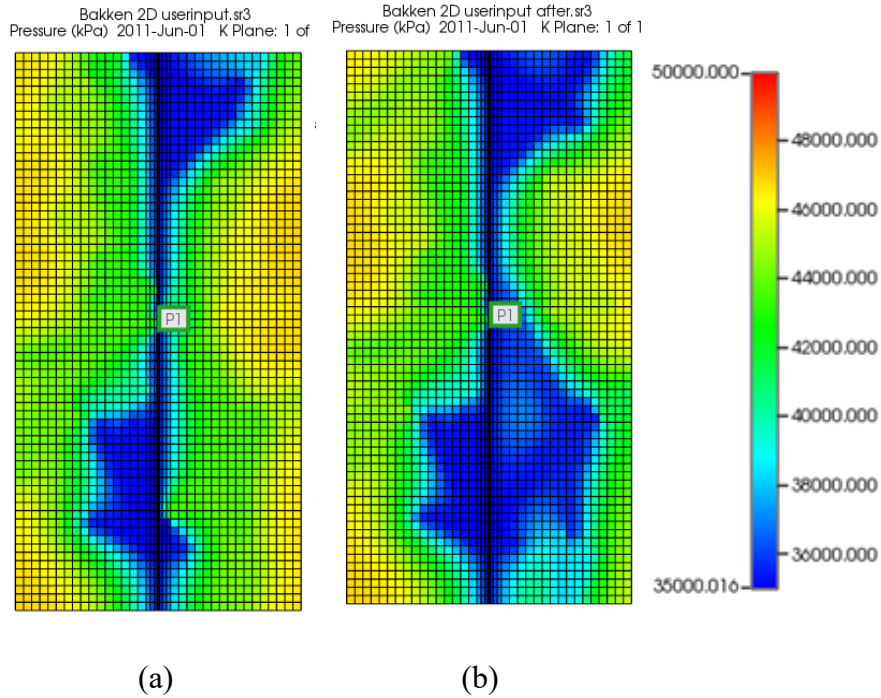
Fig. 5.3. The pressure distribution after 1734 days (4.75 years). (a) The original DPDK model;(b) the corrected DPDK model.

In this study, we also investigated the impact of the disconnection on the flowback recovery. Fig. 5.4 demonstrates the water volume in the matrix and fracture system. The graph shows the initial water volume in the matrix system is the same for the original and corrected model (Fig. 5.4(a)). However, in the fracture system, the initial water volume for the corrected model is approximately 30% greater than that for the original model (Fig. 5.4(b)). Flowback recovery is calculated as the ratio of the cumulative recovered fracture-fluid volume and the total injected fracture-fluid volume (Zhou, 2016). Some researchers have simulated fracture-fluid volumetric recovery from shale gas reservoirs during flowback periods (Clarkson and Williams-Kovacs 2013; Alkouh et al. 2014; Bertoncello et al. 2014), and the value is mostly less than 26% for a shale reservoir. In this study, the cumulative recovered fracture-fluid volume at the third week is recorded, and the flowback recovery is calculated as 5.06% for the original DPDK model; and the value increases to 10.12% for the corrected model, and the detailed calculation is shown in Appendix B. Therefore, the case

study shows the disconnection of the grid blocks has a significant impact on the calculation of flowback recovery.

(a)   (b)
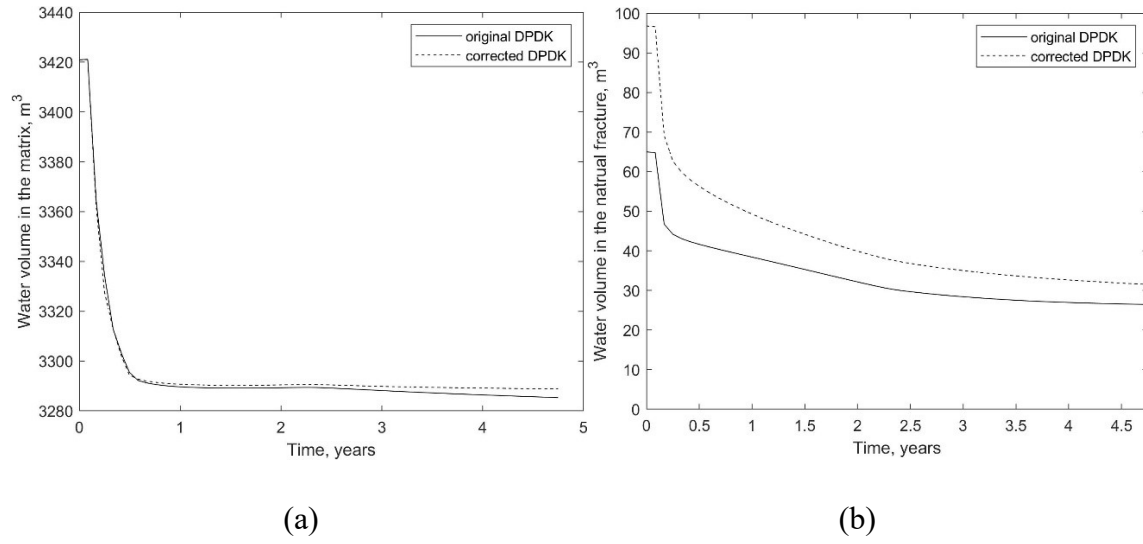
Fig. 5.4. Comparison of the water volume in the different continua. (a) Matrix; (b) fracture.

Chapter 6: Investigation of Non-Planar Twisted Hydraulic Fractures

6.1 Introduction

Most simulation models would represent a hydraulic fracture with a simplified bi-wing representation, where the fracture plane is aligned with axes on a Cartesian mesh. The bi-wing model assumes in a homogeneous and isotropic formation, a hydraulic fracture would grow along the direction of the perforation, eventually forming a bi-wing shape. Based on this assumption, KGD and PKN are the two most common bi-wing fracture geometries proposed by Khristianovic-Geertsma de Klerk (1955), Perkins and Kern (1961).

But in practice, hydraulic fracturing direction is highly influenced by the local in-situ stress, which may cause the propagation path to deviate from a plane. In some cases, if the wellbore is not oriented in the direction of any principal stress, the fracture path undulates, as it realigns itself to the plane normal to the minimum in-situ stress, and this phenomenon is called fracture twist (Jang, 2015). Fracture twist near the wellbore is regarded as highly undesirable during hydraulic fracturing, and the deformation of the fracture plane can result of high-stress anisotropy (Jin et al., 2012). The presence of twisted fractures could lead to proppant bridging, premature screenout, decreased fracture width, and increased skin (Cleary et al., 1993; Khan and Khraisheh, 2000; Jin et al., 2012). Therefore, in a horizontal well, the wells are suggested to be drilled along the minimum horizontal stress to form transverse fractures. However, in the practice, the well direction is not easy to be controlled to align with principal stresses. (Fritz et al., 1991). As a result, the phenomenon of fracture twist is common in an actual hydraulic fracturing stimulation.

Capturing these non-planar twisted fracture geometries is challenging in most commercial flow simulators, where dual-porosity dual-permeability (DKDP) models on a corner-point grid are typically used due to their computational efficiency. In principle, with an appropriate upscaling/mapping scheme, all fracture shapes can be upscaled to the DPDK model. However, the accuracy of a DPDK model decreases when simulating sparsely-distributed long fractures. Also, if the fracture planes are not aligned with the meshing orientation, the connectivity between neighboring fracture cells could be erroneously removed. In this chapter, such issues are examined and their impacts on production performance are assessed. And the proposed method is used to detect such misalignments and to adjust the DPDK fracture parameters locally to restore proper fracture connectivity, such that the fracture networks and non-planar fractures can be properly simulated in the DPDK model. In this study, the process of fracture propagation is not simulated, and it is assumed that the fracture geometry is fully formed at the initial state of the flow modeling; therefore, geomechanics effects are not coupled in the flow simulation. In this work, the fracture propagation path is generated by the process proposed by Jin et al. (2013), and the EDFM model is used to verify the accuracy of using DPDK to model these non-planar fractures.

6.2 Construction of the Fracture Path

In hydraulic fracturing, tensile and shear fracture are the two most common fracture modes. A tensile fracture occurs when minimum effective stress reduces to the tensile strength level, and shear fracture occurs when the injection pressure has a very high diffusion rate (Jin et al., 2013). The tensile fracture, also called opening mode, is usually noted as Mode I, and the shear fracture is noted as Mode II. During the fracture propagation stage, both Mode I and Mode II can occur

simultaneously. Also, the extent of each mode is represented by the stress intensity factor (SIF), which can be used to predict the stress state in the vicinity of a fracture tip caused by remote loading or residual stresses (Anderson, 2005). The expression can be represented as follows (Rice, 1968a; Barry et al., 1992):

$$K_I = (P - \sigma_H \sin^2 \beta - \sigma_h \sin^2 \beta)\sqrt{\pi a} , \tag{6.1}$$

$$K_{II} = \frac{1}{2}(\sigma_H - \sigma_h)\sin 2\beta \sqrt{\pi a} . \tag{6.2}$$

K_I and K_{II} represent the SIF of opening mode and shear mode respectively; P is the fluid pressure inside fracture; σ_H is the maximum horizontal in-situ stress; σ_h is the minimum horizontal in-situ stress; a represents the preexisting fracture length which is perpendicular to the horizontal well, and β is the inclination angle which is defined as the angle between the direction of horizontal well and minimum horizontal in-situ principal stress. A schematic of a twisted fracture with the inclination angle of β and pre-existing fracture length of a is shown in Fig. 6.1.
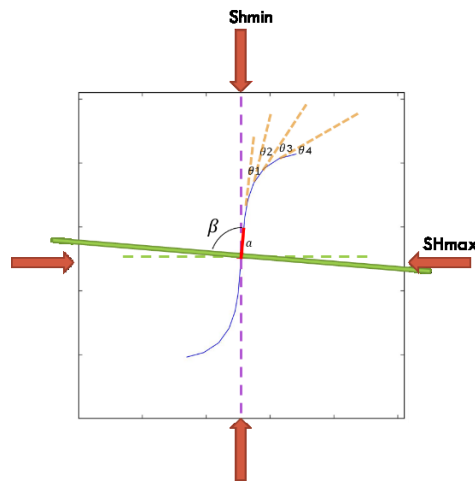
Fig. 6.1. Schematic of the reorientation of the hydraulic fracture in response to the varying in-situ stress (The blue curved line represents the fracture path, the red short solid line denotes the pre-existing fracture, and the green solid line represents the horizontal well).

For different inclination angles, different stress exerts on the hydraulic fracture and different modes dominate the propagation mechanisms. SIF ratio represents how much the fracture propagation is affected by the opening mode type when both exist, and its expression is defined as K_I/K_{II}. The higher the SIF ratio, the more the fracture propagation is affected by the opening mode, and in this situation, the fracture will not twist much and tend to grow along its current direction. Conversely, the lower the SIF ratio, the fracture propagation will be dominated by the shear mode, and there will be more likelihood of the fracture twist.

After calculating the SIFs, fracture initiation angle can be predicted with proper fracture propagation criteria. The initiation θ_m angle represents the angle between the current and future fracture propagation direction. The initiation angle of each step plays an important role in determining the propagation path. According to the maximum tangential stress criterion, which is also noted as σ_θ-Criterion (Erdogan and Sih, 1963), the initiation angle at each step can be expressed as (Jin et al., 2013):

$$\theta_m = 2\arctan[\frac{1}{4}\frac{K_I}{K_{II}} - \frac{1}{4}\sqrt{(\frac{K_I}{K_{II}})^2 + 8}]. \qquad (6.3)$$

The value of θ_m varies in different inclination angles. With the given parameters in Table. 6.1, the relationship between the initiation angle and the inclination (β) angle roughly follows the pattern shown in Fig. 6.2. It can be observed that for $\beta > 50$ degrees, θ_m increases with β, while for $\beta < 50$ degrees, θ_m decreases with β. The fracture path is divided into n smaller segments. To generate the entire fracture path, the following algorithm is used to compute β for each segment:

Step 1: calculate the KI and KII from Eq. (6.1) and (6.2);

Step 2: substitute the value of KI and KII in Eq. (6.3) to get the θ_{mi};

Step 3: update the value of β in Eq. (6.1) and Eq. (6.2) with $\beta_i + \sum_{i=1}^{n} \theta_{mi}$ for the nth small fracture segment;

Step 4: repeat from step 1.

The fracture path direction changes within the propagation and the pattern is shown in Figure. 6.3. In this study, we assume the same amount of fracture fluid is injected into the reservoir to create the hydraulic fracture, and the fracture length for each twisted fracture is the same.

Table. 6.1. Essential parameters for fracture path generation.

Parameters	Values	Units
Maximum horizontal stress	20	MPa
Minimum horizontal stress	15	MPa
Preexisting fracture length	3	m
Poisson's ratio	0.25	
Fluid pressure inside fracture	35	MPa
Growing length for each step	5	m
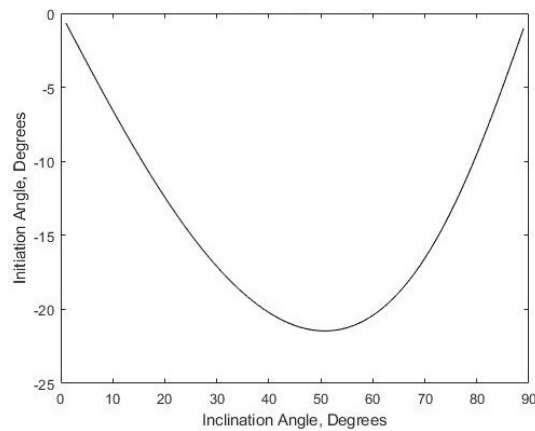
Fig. 6.2. Change of initiation angle with different inclination angles.
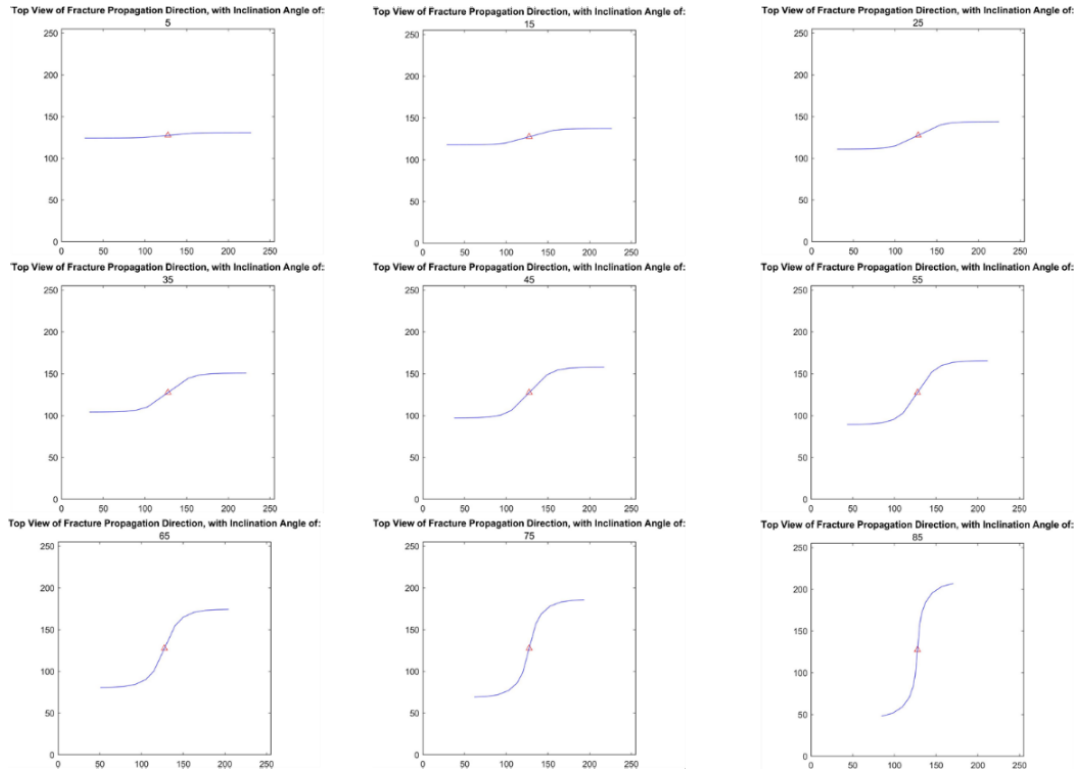
Fig. 6.3. Generated fracture path based on σθ-Criterion.

6.3 Flow Simulation of a Non- Planar Twisted Fracture

The geometry of non-planar twisted fractures cannot be explicitly expressed in most flow simulators with corner-pointed meshing. However, in the DPDK method, by upscaling the DFN to the equivalent DPDK model, discrete fractures can be represented implicitly and structured meshing can still be implemented. The EDFM model, on the other hand, which has been introduced in the Chpater 4, fractures are embedded within a cell, and it can also handle the non-planar fractures. Since the more sophisticated EDFM is capable of capturing the flow in complex geometries, the production profile of the EDFM model is used to examine the improvement of the accuracy of the DPDK model after correction.

6.3.1 DPDK Flow Simulation

The accuracy of using DPDK to simulate the long fractures is sometimes concerned. For the purpose of validating the accuracy of the DPDK model for this specific study, two sets of different mesh resolution are constructed and the meshing information is shown in Table. 6.2. And the reservoir model is simulated by using the same reservoir properties in Table. 4.1. Nine non-planar fractures shown in Fig. 6.3 are generated and loaded to FracMan® and Oda's method is applied to upscale the fractures to the DPDK model for two different meshes.

The result of the oil production rate for the fine mesh is shown in Fig. 6.4(a) and the coarse mesh is shown in Fig. 6.4(b). Substantial differences can be observed among these profiles corresponding to different inclination angles. Fig. 6.5 compares the fracture effective permeability before and after correction. Some disconnections can be easily detected in Fig. 6.5(a), and after all missing DPDK parameters are corrected, the fracture configuration is shown in Fig. 6.5(b). The oil production rate of the corrected DPDK model for both the fine mesh and coarse mesh shows a significant change in Fig. 6.6: the difference between curves is dramatically reduced, and most are overlapped after a 0.5-year production.

Table. 6.2. Dimension and meshing scheme of two different levels of refinement.

Name	Dimension	Meshing scheme
Coarse grid	305×255×5	61×51×1
Fine grid	305×255×5	97×81×1
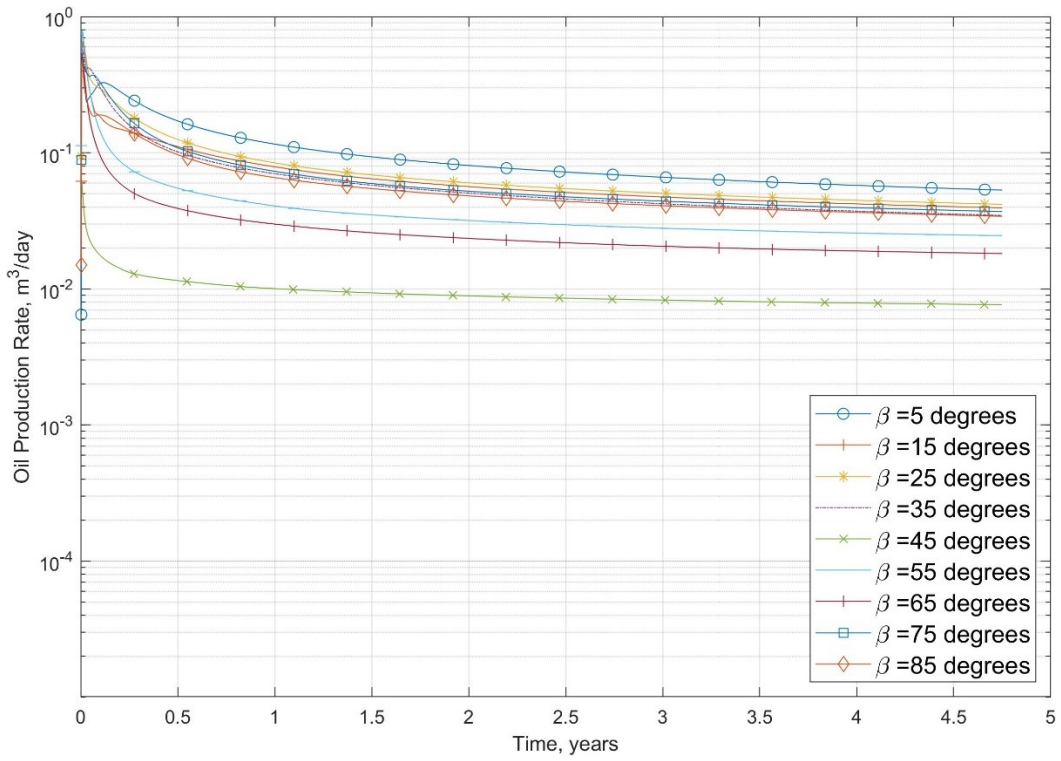
(a)
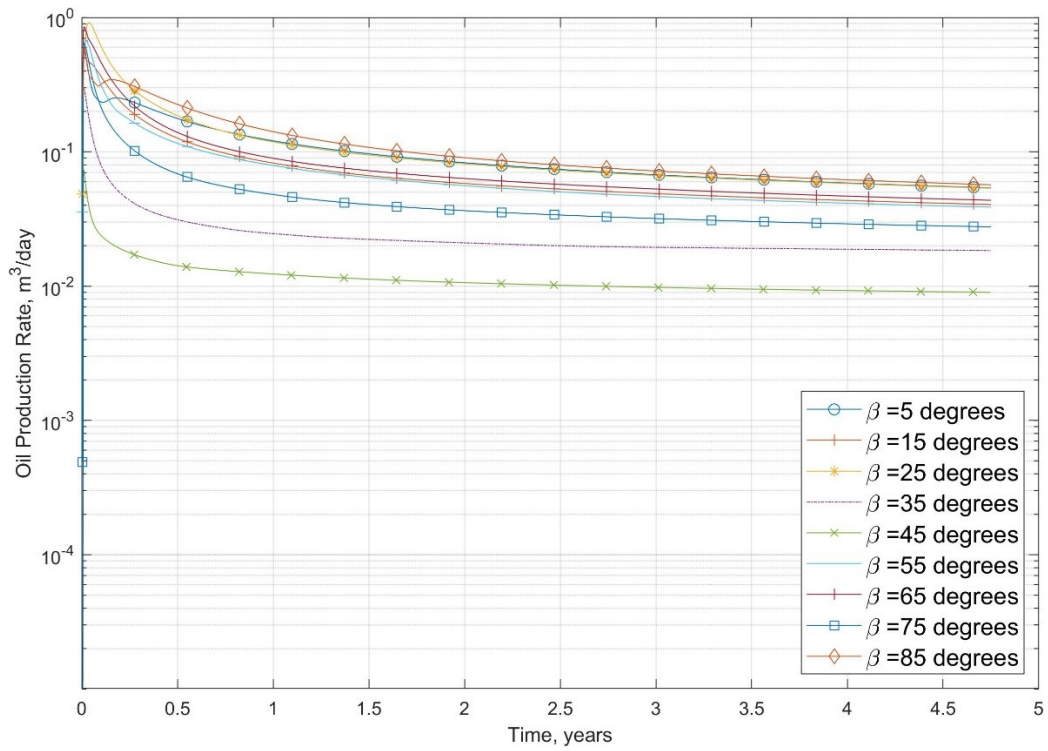
(b)

Fig. 6.4. Comparison of oil production rate of the original DPDK model. (a) Fine mesh; (b) coarse mesh.
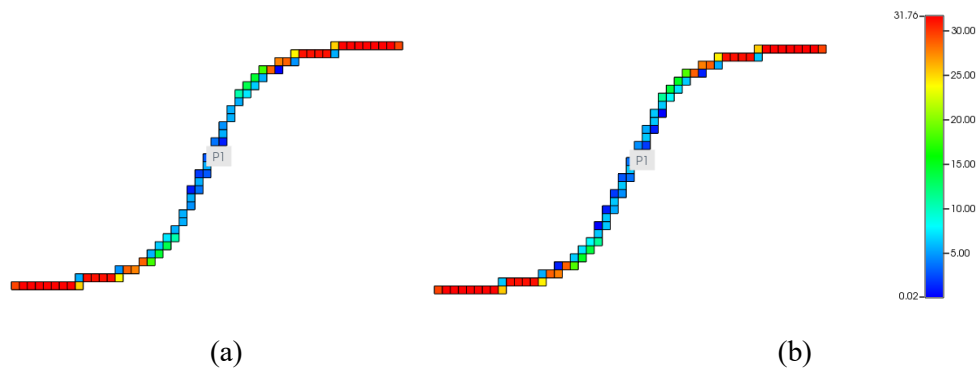
Fig. 6.5. The effective fracture permeability of a fracture with an inclination angle of 65 degrees. (a) Original DPDK model; (b) connected DPDK model.

(a)
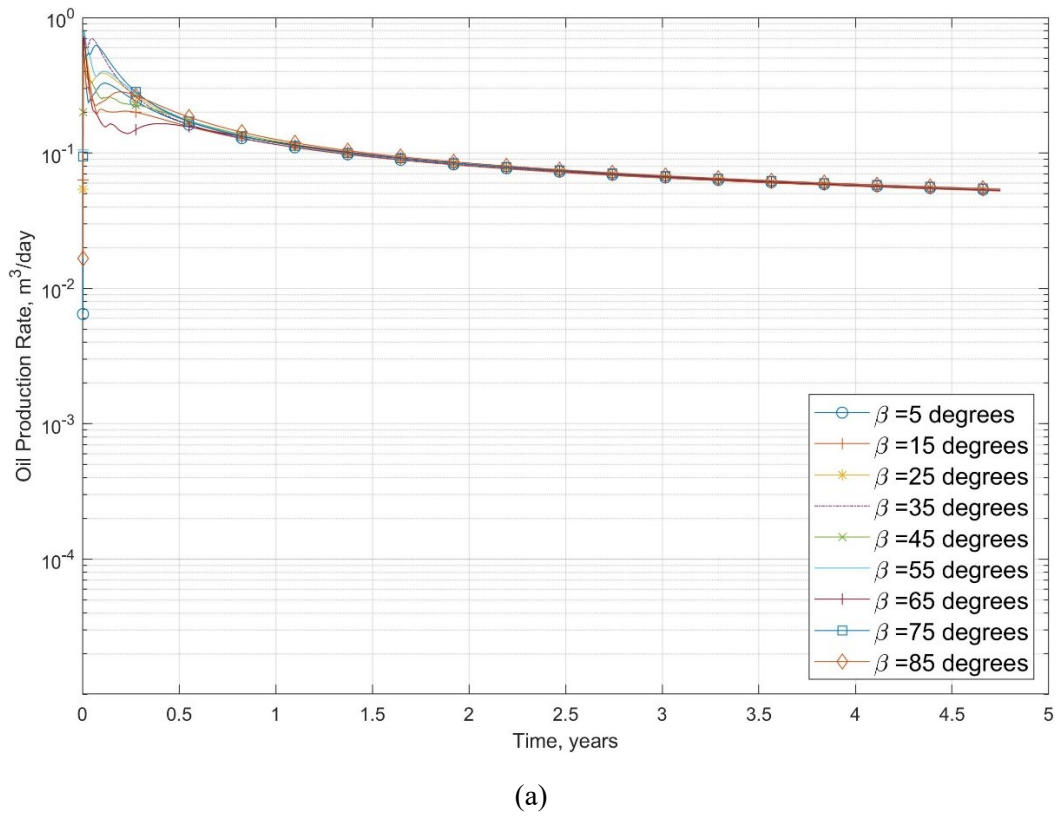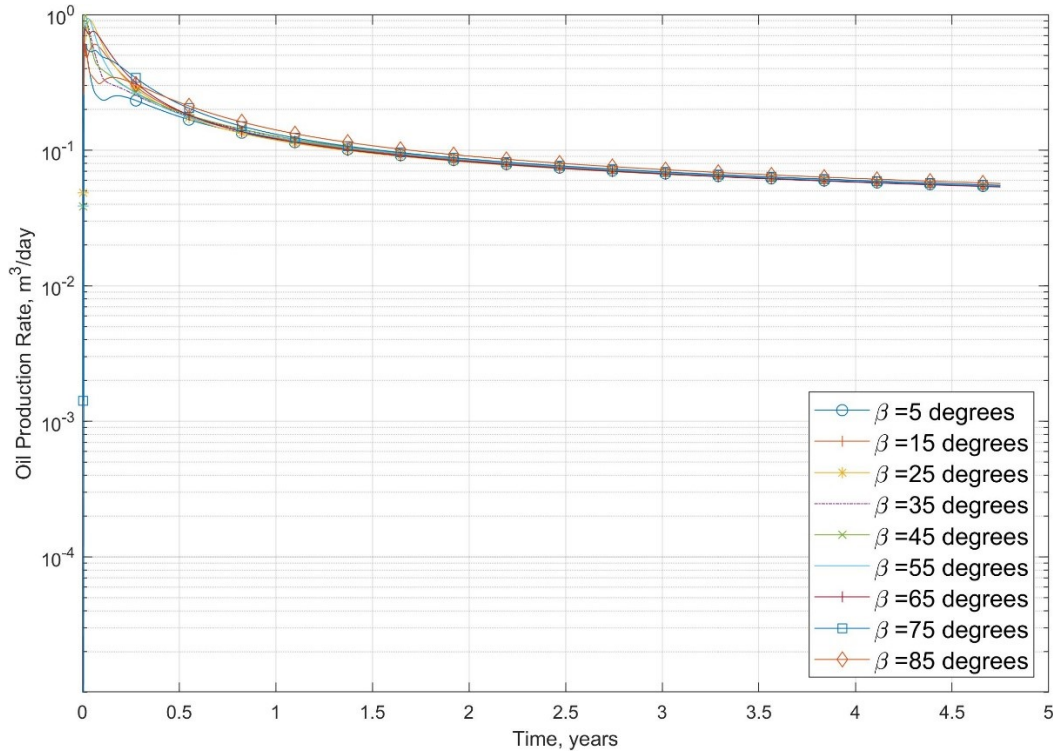
Fig. 6.6. Comparison of oil production rate of the corrected DPDK model. (a) Fine mesh; (b) coarse mesh.

6.3.2 Comparison with the EDFM

An EDFM model is constructed with the same reservoir and fracture parameters as the DPDK model. As an example, the fracture grid and the fracture-fracture NNCs for a twisted fracture with an inclination angle of 45 degrees are shown in Fig. 6.7. From the simulation results of the EDFM model, it can be observed the production profile for the fractures with different inclination angles are almost overlapping (Fig. 6.8). The result implies that if the fracture length remains constant, the specific orientation or inclination may not significantly affect the production profile if the effect of the geomechanics (e.g., fracture closure) is not included.

Finally, results for the EDFM and DPDK models (both original and corrected) are compared in Fig. 6.9. It can be observed that the corrected DPDK model can dramatically increase the accuracy

of the simulation results when compared against the more precise EDFM modelling. The comparison between the simulation result of the DPDK and EDFM model verifies that if the fractures or the DFNs are upscaled appropriately, the DPDK model is capable of simulating the sparsely distributed non-planar fractures. There is a noticeable improvement in the production performance after restoring the connectivity between those previously disconnected cells. In other words, ignoring the impacts of mesh discretization could result in an unintended reduction in the simulated fracture connectivity and a considerable underestimation of the cumulative production and SRV estimation. Also, the adjusted model can successfully represent different fracture inclination angle with different propagation paths.

(a)   (b)
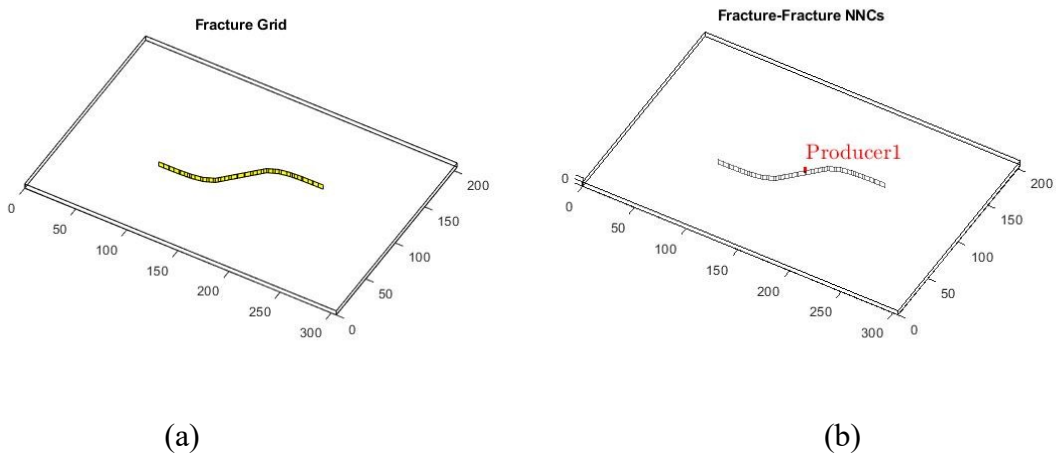
Fig. 6.7. Schematics of a twisted fracture with an inclination angle of 45 degrees. (a) Fracture grid; (b) Fracture-fracture NNCs.
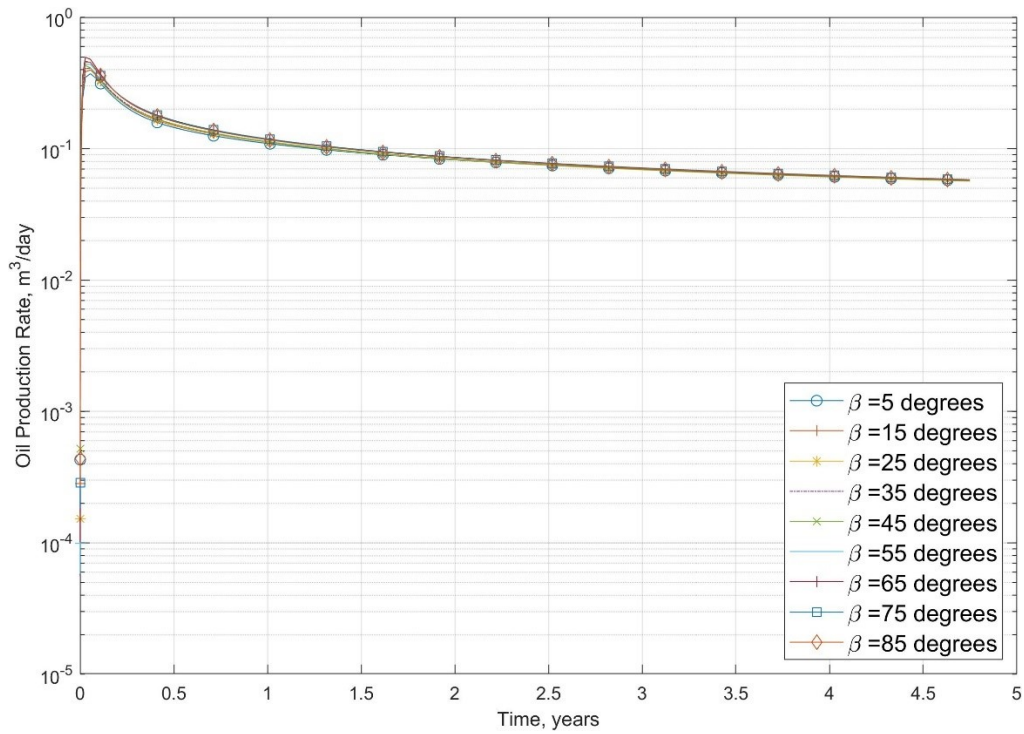
Fig. 6.8. Oil production rate profiles for different values of β predicted using the EDFM model.
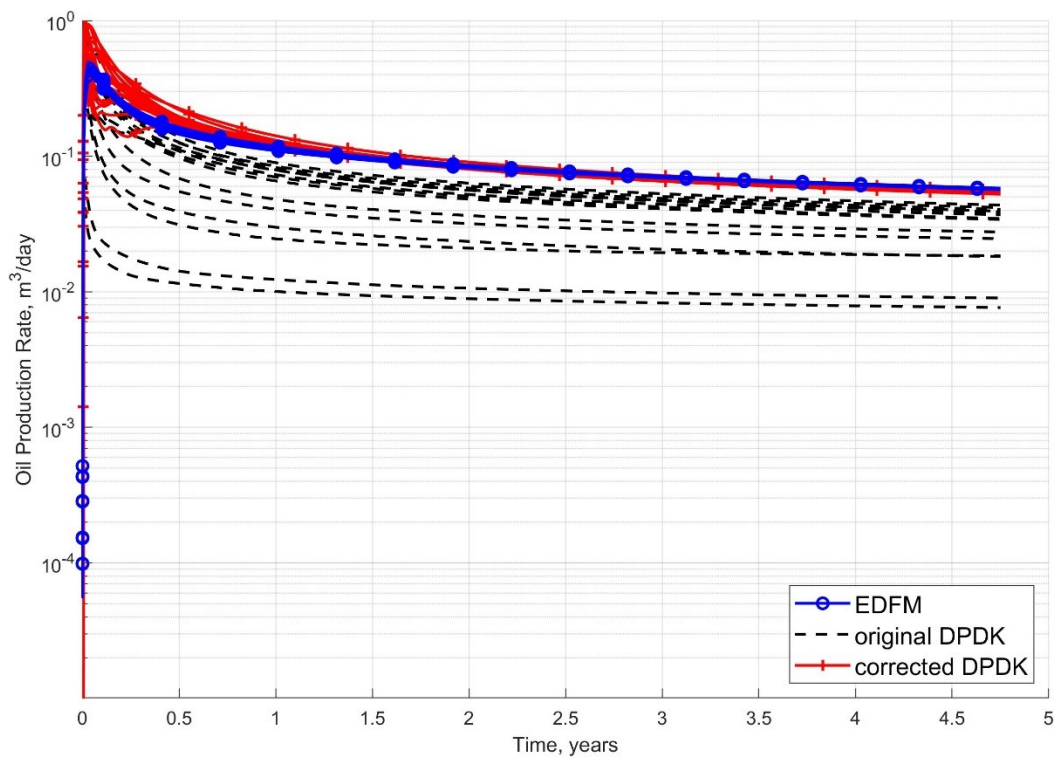
Fig. 6.9. Comparison of oil production rate of the EDFM model, original and corrected DPDK model.

Chapter 7: Conclusions and Future Works

7.1 Conclusions

1. Structured meshes and dual-porosity dual-permeability (DPDK) models are commonly used to simulate flow in fractured systems. This approach is generally acceptable for systems with high fracture intensity, or systems with very low fracture intensity, as any errors associated with the mesh discretization, are likely to be insignificant. However, for unconventional reservoirs, the reality often lies between the two extremes, rendering the connectivity between neighboring fracture cells to be erroneously removed when the fracture plane is not aligned along the meshing direction. This study quantitatively demonstrates the impact of such misalignments and the negative impacts on production due to the disconnected fracture cells.

2. A detection scheme is implemented to identify these disconnected fracture cells, and a correction scheme is used to re-establish the necessary connection.

3. Simulation results of the corrected DPDK models are closer to those of single-porosity DFN and EDFM simulations. There is a noticeable improvement in the production after restoring the connectivity between those previously disconnected cells.

4. The misalignment and number of missing fracture cells increase with mesh refinement, medium level of fracture density, and fracture trend angle.

5. Although two different options are offered to correct the missing connections, there is little difference in the simulation results for these two correction methods. This observation suggests that restoring the missing connection is more important than the specific values being assigned to the fracture cells.

6. In the study of the soaking period and the flow back process. The result shows ignoring the impacts of mesh discretization could result in a considerable underestimation of the cumulative production and SRV estimation. And the result could have a significant impact on the fracture fluid recovery calculation.

7. In simulating the non-planar fractures, a noticeable improvement is shown in the production performance after restoring the connectivity between those previously disconnected cells. In other words, with a correction on the non-planar fractures, the adjusted model can successfully represent different fracture inclination angle and a variety of propagation paths.

8. Considering that upscaling a DFN to a DPDK model is still a commonly adopted simulation approach, the insights presented in this paper provides a convenient way to enhance the accuracy of the upscaled model significantly. There is a noticeable improvement in the production after restoring the connectivity between those previously disconnected cells. Ignoring the impacts of mesh discretization or misalignment could lead to an unintended reduction in fracture connectivity, total stimulated volume, and oil production.

7.2 Future Works

1. Structured meshing has an inherent limitation of describing the details of the fractures. The flow that cannot go through the diagonal direction is just one of the drawbacks. The unstructured meshing is more suitable to describe the fractures with complex structures. In future work, more sophisticated DFN in unstructured meshing will be investigated to study the NFRs.

2. Oda's method does not count for the fractures with very low density. In future work, we will try the proposed the corrected Oda's method (Haridy, 2019), which accounts for the fracture connectivity and length. And it is worth showing the difference in the simulation result between the DPDK model applied with the corrected Oda's method and the DPDK corrected method proposed in this thesis.

3. Flow-based upscaling is considered more accurate than analytical upscaling. The flow-based upscaling could capture the pressure and saturation change within the matrix and provide more details of the fractures. In future works, flow-based upscaling like MSR should be investigated to combine with DPDK flow simulation. And it is interesting to show the difference in the result between the flow-based upscaling method and the corrected upscaling method proposed in the thesis.

4. In this study, we investigated the simulation of non-planar fractures using the DPDK method. But the study did not include the effects of geomechanics. A more legalistic model should consider the stress change in the reservoir, especially for the non-planar fractures dominated by the stress from many directions. Therefore, in future work, I will couple geomechanics in simulating the non-planar fractures, study the local in-situ stress change around the fractures, and analyze the difference in production performance caused by the change of in-situ stress for fractures with different inclination angles.

5. In this study, the illustrated tight oil case studies were constructed based on the black-oil model with only water-oil two-phase flow. However, in shale exploration, the mainly produced hydrocarbon from the formation is the gas. Therefore, in future work, I will incorporate the gas in the unconventional reservoir simulations by using the DPDK model, in which non-Darcy flow mechanisms including slippage effect, Knudsen diffusion and adsorption need to be considered.

6. In this study, the reservoir model has a uniform distribution of reservoir parameters like permeability and porosity. However, in the low permeable formations, the reservoir heterogeneity will cause phase and composition change. Therefore, in future work, I will consider the reservoir heterogeneity and use the compositional model to capture the composition change and other phase behaviors in the model.

Bibliography

Acock, A., ORourke, T., Shirmboh, D., Alexander, J., Andersen, G., Kaneko, T., ... & Twynam, A. (2004). Practical approaches to sand management. Oilfield review, 16(1), 10-27.

Ahmed Elfeel, M. (2014). Improved upscaling and reservoir simulation of enhanced oil recovery processes in naturally fractured reservoirs (Doctoral dissertation, Heriot-Watt University).

Akram, A. H., Gherryo, Y. S., Ali, M., Thabt, M. S., & Serban, A. (2010, January). Dynamic behavior of a fissured dual-carbonate reservoir modeled with DFN. In North Africa Technical Conference and Exhibition. Society of Petroleum Engineers.

Anderson, T. L. (2005), Fracture mechanics: fundamentals and applications, 3rd ed., CRC Press.

Rice, J. R. (1968a), Mathematical analysis in the mechanics of fracture, Fracture: An advanced treatise, 2, 191-311.

Barry, N., N. R. Whittaker, and S. G. Singh (1992), Rock fracture mechanics principles design and applications, ELSEVIER, Amsterdam-London-New York-Tokyo.

Bianch, L. (1968). Permeability of crystalline rock interpreted from measured orientations and apertures of fractures. Analysis of Acid Zone, 8(2), 231-245.

Blaskovich, F. T., Cain, G. M., Sonier, F., Waldren, D., & Webb, S. J. (1983, January). A multicomponent isothermal system for efficient reservoir simulation. In Middle east oil technical conference and exhibition. Society of Petroleum Engineers.

Chen, Z., Huan, G., & Ma, Y. (2006). Computational methods for multiphase flows in porous media. Society for Industrial and Applied Mathematics.

Cheng, Y. (2012). Impact of water dynamics in fractures on the performance of hydraulically fractured wells in gas-shale reservoirs. Journal of Canadian Petroleum Technology, 51(02), 143-151.

Clarkson, C. R., Williams-Kovacs, J., Zhang, Z., Yuan, B., Ghanizadeh, A., Hamdi, H., & Islam, A. (2020, September). Case Studies of Integrated Flowback Analysis: Examples from the Montney

and Duvernay Formations. In SPE Canada Unconventional Resources Conference. Society of Petroleum Engineers.

Cleary, M. P., Johnson, D. E., Kogsbøll, H. H., Owens, K. A., Perry, K. F., De Pater, C. J., ... & Mauro, T. (1993, January). Field implementation of proppant slugs to avoid premature screen-out of hydraulic fractures with adequate proppant concentration. In Low permeability reservoirs symposium. Society of Petroleum Engineers.

Cottereau, N., Garcia, M. H., Gosselin, O. R., & Vigier, L. (2010, January 1). Effective Fracture Network Permeability: Comparative Study of Calculation Methods. In SPE EUROPEC/EAGE Annual Conference and Exhibition, Barcelona, Spain, June 14-17.

Cornette, B. M., Telker, C., & De La Pena, A. (2012, February). Refining discrete fracture networks with surface microseismic mechanism inversion and mechanism-driven event location. In SPE Hydraulic Fracturing Technology Conference. The Woodlands, Texas, USA, February.

Cui, T., Wang, K., Liu, H., Luo, J., & Chen, Z. (2016, October 25). Efficient and Scalable Methods for Dual-Porosity/Permeability Models in Fractured Reservoir Simulations. In SPE Asia Pacific Oil & Gas Conference and Exhibition, Perth, Australia, October 25-27.

Dershowitz, B., LaPointe, P., Eiben, T., & Wei, L. (2000). Integration of discrete feature network methods with conventional simulator approaches. SPE Reservoir Evaluation & Engineering, 3(02), 165-170.

Ding, D. Y., Farah, N., Bourbiaux, B., Wu, Y. S., & Mestiri, I. (2018). Simulation of matrix/fracture interaction in low-permeability fractured unconventional reservoirs. SPE Journal, 23(04), 1-389.

Dong, Z., Li, W., Lei, G., Wang, H., & Wang, C. (2019). Embedded discrete fracture modeling as a method to upscale permeability for fractured reservoirs. Energies, 12(5), 812.

Durlofsky, L. J. (2005, June). Upscaling and gridding of fine scale geological models for flow simulation. In 8th International Forum on Reservoir Simulation Iles Borromees, Stresa, Italy (Vol. 2024, pp. 1-59).

Energy Information Administration (US) (Ed.). (2020). Annual Energy Outlook 2020. Government Printing Office.

Erdogan, F., and G. Sih (1963), On the crack extension in plates under plane loading and transverse shear, Journal of Basic Engineering, 85, 519.

Ertekin, T., Abou-Kassem, J. H., & King, G. R. (2001). Basic applied reservoir simulation (Vol. 7). Richardson, TX: Society of Petroleum Engineers.

Fakcharoenphol, P., Torcuk, M. A., Bertoncello, A., Kazemi, H., Wu, Y. S., Wallace, J., & Honarpour, M. (2013, September). Managing shut-in time to enhance gas flow rate in hydraulic fractured shale reservoirs: a simulation study. In SPE Annual Technical Conference and Exhibition. Society of Petroleum Engineers.

Fan, L., Thompson, J. W., & Robinson, J. R. (2010, January). Understanding gas production mechanism and effectiveness of well stimulation in the Haynesville Shale through reservoir simulation. In Canadian unconventional resources and international petroleum conference. Society of Petroleum Engineers.

Fritz, R. D., M. K. Horn, and S. D. Joshi (1991), Geological aspects of horizontal drilling, The American Association of Petroleum Geologists, Tulsa, Oklahoma, USA.

Fumagalli, A., Pasquale, L., Zonca, S., & Micheletti, S. (2016). An upscaling procedure for fractured reservoirs with embedded grids. Water Resources Research, 52(8), 6506-6525.

Ghahfarokhi, P. K. (2017). The structured gridding implications for upscaling model discrete fracture networks (DFN) using corrected Oda's method. Journal of Petroleum Science and Engineering, 153, 70-80.

Gilman, J. R. (1986). An efficient finite-difference method for simulating phase segregation in the matrix blocks in double-porosity reservoirs. SPE Reservoir Engineering, 1(04), 403-413.

Hajibeygi, H., Karvounis, D., & Jenny, P. (2011). A hierarchical fracture model for the iterative multiscale finite volume method. Journal of Computational Physics, 230(24), 8729-8743.

Haridy, M. G., Sedighi, F., Ghahri, P., Ussenova, K., & Zhiyenkulov, M. (2019, October). Comprehensive Study of the Oda Corrected Permeability Upscaling Method. In SPE/IATMI Asia Pacific Oil & Gas Conference and Exhibition, Bali, Indonesia, October 29-31.

Hill, A. C., & Thomas, G. W. (1985, January). A new approach for simulating complex fractured reservoirs. In Middle east oil technical conference and exhibition. Society of Petroleum Engineers.

Hoeink, T., Stoddard, T., & Ben, Y. (2016, June). Directional Equivalent Permeability of Discrete Fracture Networks. In 50th US Rock Mechanics/Geomechanics Symposium. American Rock Mechanics Association.

Hu, Z. Q., Long, J. H., & Wang, X. J. (2014). Self-healing, natural restoration and artificial restoration of ecological environment for coal mining. Journal of China Coal Society, 39, 1751-1757.

Hui, M. H., Gong, B., Karimi-Fard, M., & Durlofsky, L. J. (2007, January). Development and application of new computational procedures for modeling miscible gas injection in fractured reservoirs. In SPE Annual Technical Conference and Exhibition, Anaheim, California, U.S.A, November 11-14.

Hui, M.-H., Mallison, B. T., Fyrozjaee, M. H., & Narr, W. (2013, September 30). The Upscaling of Discrete Fracture Models for Faster, Coarse-Scale Simulations of IOR and EOR Processes for Fractured Reservoirs. In SPE Annual Technical Conference and Exhibition, New Orleans, Louisiana, USA, September 30 – October 2.

Hui, M. H., Dufour, G., Vitel, S., Muron, P., Tavakoli, R., Rousset, M., ... & Mallison, B. (2019, March). A robust embedded discrete fracture modeling workflow for simulating complex processes in field-scale fractured reservoirs. In SPE Reservoir Simulation Conference. OnePetro.

Jang, Y., Kim, J., Ertekin, T., & Sung, W. M. (2015, October). Modeling multi-stage twisted hydraulic fracture propagation in shale reservoirs considering geomechanical factors. In SPE eastern regional meeting. Society of Petroleum Engineers.

Jiang, J., & Younis, R. M. (2017). An improved projection-based embedded discrete fracture model (pEDFM) for multiphase flow in fractured reservoirs. Advances in water resources, 109, 267-289.

Jin, X., S. Shah, and M. Sheng (2012), Hydraulic fracturing model based on nonlinear facture mechanics: theory and simulation, paper presented at SPE Annual Technical Conference and Exhibition, San Antonio, Texas, USA, October 8 -10.

Jin, X., S. Shah, J. Roegiers, and B. Hou (2013), Breakdown Pressure Determination-A Fracture Mechanics Approach, paper presented at SPE Annual Technical Conference and Exhibition, New Orleans, Louisiana, USA, Sep 30 - Oct 2.

Karimi-Fard, M., Durlofsky, L. J., & Aziz, K. (2004). An efficient discrete-fracture model applicable for general-purpose reservoir simulators. SPE journal, 9(02), 227-236.

Kazemi, H., Seth, M. S., & Thomas, G. W. (1969). The interpretation of interference tests in naturally fractured reservoirs with uniform fracture distribution. Society of Petroleum Engineers Journal, 9(04), 463-472.

Kazemi, H., Merrill Jr, L. S., Porterfield, K. L., & Zeman, P. R. (1976). Numerical simulation of water-oil flow in naturally fractured reservoirs. Society of Petroleum Engineers Journal, 16(06), 317-326.

Khan, S. M., & Khraisheh, M. K. (2000). Analysis of mixed mode crack initiation angles under various loading conditions. Engineering Fracture Mechanics, 67(5), 397-419.

Khristianovic, S.A., Zheltov, Y.P. (1955). Formation of vertical fractures by means of highly viscous liquid. Proceedings of the 4th World Petroleum Congress, Rome, pp. 579–586

Kumar, S., Rey, A., Dufour, G., & Ogunyomi, B. (2019, September 23). Understanding Fluid Flow Behavior in Fractured Reservoir using Dual Porosity Dual Permeability and Discretized Fracture Model. SPE Annual Technical Conference and Exhibition, Calgary, Alberta, Canada, September 30 – October 2.

Lee, S. H., Lough, M. F., & Jensen, C. L. (2001). Hierarchical modeling of flow in naturally fractured formations with multiple length scales. Water resources research, 37(3), 443-455.

Li, L., & Lee, S. H. (2008). Efficient field-scale simulation of black oil in a naturally fractured reservoir through discrete fracture networks and homogenized media. SPE Reservoir Evaluation & Engineering, 11(04), 750-758.

Li, G., Guo, B., Li, J., & Wang, M. (2019). A Mathematical Model for Predicting Long-Term Productivity of Modern Multifractured Shale-Gas/Oil Wells. SPE Drilling & Completion, 34(02), 114-127.

Li, J., Liu, Y., Xue, L., Cheng, Z., Kong, X., & Li, S. (2019, November). Flowback Analysis of Complex Fracture Networks in the Unconventional Reservoir Using Finite Element Method with Coupled Flow and Geomechanics. In Abu Dhabi International Petroleum Exhibition & Conference. Society of Petroleum Engineers.

Lie, Knut-Andreas. 2019. An introduction to reservoir simulation using MATLAB/GNU Octave: User guide for the MATLAB Reservoir Simulation Toolbox (MRST): Cambridge University Press.

Liu, Y., Leung, J.Y., Chalaturnyk, R., and Virues, C.J.J. (2019). New insights on mechanisms controlling fracturing fluid distribution and its impacts on well performance in shale gas reservoirs. SPE Production & Operations 34(3): 564-585.

Liu, Y., Liu, L., Leung, J.Y., Wu, K., and Moridis, G.J. (accepted). Coupled flow and geomechanics modeling of inter-fracture water injection to enhance oil recovery in tight reservoirs. SPE Journal.

Moinfar, A., Narr, W., Hui, M. H., Mallison, B. T., & Lee, S. H. (2011, January). Comparison of discrete-fracture and dual-permeability models for multiphase flow in naturally fractured reservoirs. In Spe reservoir simulation symposium. Society of Petroleum Engineers.

Moinfar, A., Varavei, A., Sepehrnoori, K., & Johns, R. T. (2012, January 1). Development of a Novel and Computationally-Efficient Discrete-Fracture Model to Study IOR Processes in Naturally Fractured Reservoirs. In SPE Improved Oil Recovery Symposium, Tulsa, Oklahoma, USA, April 14-18.

Moinfar, Ali, Varavei, Abdoljalil, Sepehrnoori, Kamy, Johns, Russell T., 2014. Development of an efficient embedded discrete fracture model for 3D compositional reservoir simulation in fractured reservoirs. SPE Journal. 19 (02), 289–303.

Nejadi, S., Leung, J.Y., Trivedi, J.J., and Virues, C. (2015). Integrated characterization of hydraulically fractured shale gas reservoirs – production history matching. SPE Reservoir Evaluation & Engineering 18(4): 482-494.

Nejadi, S., Trivedi, J. J., & Leung, J. (2017). History matching and uncertainty quantification of discrete fracture network models in fractured reservoirs. Journal of Petroleum Science and Engineering, 152, 21-32.

Noorishad, J., & Mehran, M. (1982). An upstream finite element method for solution of transient transport equation in fractured porous media. Water Resources Research, 18(3), 588-596.

Oda, M. A. S. A. N. O. B. U. (1985). Permeability tensor for discontinuous rock masses. Geotechnique, 35(4), 483-495.

Panfili, P., & Cominelli, A. (2014, November 10). Simulation of Miscible Gas Injection in a Fractured Carbonate Reservoir using an Embedded Discrete Fracture Model. In Abu Dhabi International Petroleum Exhibition and Conference, Abu Dhabi, UAE, November 10-13.

Pruess, K. (1985). A practical method for modeling fluid and heat flow in fractured porous media. Society of Petroleum Engineers Journal, 25(01), 14-26.

Perkins, T. K., & Kern, L. R. (1961). Widths of hydraulic fractures. Journal of Petroleum Technology, 13(09), 937-949.

Rossen, R. H. (1977). Simulation of naturally fractured reservoirs with semi-implicit source terms. Society of Petroleum Engineers Journal, 17(03), 201-210.

Rutledge, J. T., Downie, R. C., Maxwell, S. C., & Drew, J. E. (2013, September). Geomechanics of hydraulic fracturing inferred from composite radiation patterns of microseismicity. In SPE Annual Technical Conference and Exhibition. Society of Petroleum Engineers.

Sarda, S., Jeannin, L., & Bourbiaux, B. (2001, January 1). Hydraulic Characterization of Fractured Reservoirs: Simulation on Discrete Fracture Models. SPE Reservoir Simulation Symposium, Houston, Texas, February 11-14.

Shaibu, R., & Guo, B. (2020, October). A Data-Driven Water-Soaking Model for Optimizing Shut-In Time of Shale Gas/Oil Wells Prior to Flowback of Fracturing Fluids. In SPE Annual Technical Conference and Exhibition. Society of Petroleum Engineers.

Shaoul, J. R., Van Zelm, L. F., & De Pater, H. J. (2011, January). Damage mechanisms in unconventional gas well stimulation-A new look at an old problem. In SPE Middle East Unconventional Gas Conference and Exhibition. Society of Petroleum Engineers.

Sherratt, J., Haddad, A. S., Rafati, R., & Manzari, M. T. (2020). A fracture upscaling method (FUM) for hydraulically fractured reservoirs: From discrete fracture modelling to finite difference simulations. Journal of Natural Gas Science and Engineering, 83, 103611.

Shiozawa, S., & McClure, M. (2016). Simulation of proppant transport with gravitational settling and fracture closure in a three-dimensional hydraulic fracturing simulator. Journal of Petroleum Science and Engineering, 138, 298-314.

Sun, J., & Schechter, D. S. (2014, October 27). Optimization-Based Unstructured Meshing Algorithms for Simulation of Hydraulically and Naturally Fractured Reservoirs with Variable Distribution of Fracture Aperture, Spacing, Length and Strike. In SPE Annual Technical Conference and Exhibition, Amsterdam, The Netherlands, October 27-29.

Tene, M., Bosma, S. B., Al Kobaisi, M. S., & Hajibeygi, H. (2017). Projection-based embedded discrete fracture model (pEDFM). Advances in Water Resources, 105, 205-216.

Thomas, L. K., Dixon, T. N., & Pierson, R. G. (1980, January). Fractured reservoir simulation. In SPE Annual Technical Conference and Exhibition. Society of Petroleum Engineers.

Uleberg, K., & Kleppe, J. (1996). Dual porosity, dual permeability formulation for fractured reservoir simulation. In Norwegian university of science and technology, trondheim RUTH seminar, stavanger.

Van Heel, A. P., Boerrigter, P. M., & van Dorp, J. J. (2008). Thermal and hydraulic matrix-fracture interaction in dual-permeability simulation. SPE Reservoir Evaluation & Engineering, 11(04), 735-749.

Vavryčuk, V. (2015). Inversion for the composite moment tensor. Bulletin of the Seismological Society of America, 105(6), 3024-3035.

Vitel, S. and Souche, L. 2007. Unstructured Upgridding and Transmissibility Upscaling for Preferential Flow Paths in 3D Fractured Reservoirs. In SPE Reservoir Simulation Symposium, Houston, February 26-28.

Wang, C., & Zeng, Z. (2011, January). Overview of geomechanical properties of Bakken formation in Williston Basin, North Dakota. In 45th US Rock Mechanics/Geomechanics Symposium. American Rock Mechanics Association.

Wang, K., Peng, X., Du, Z., Haghighi, M., & Sayyafzadeh, M. (2015, November). DFN Model for Flow Simulation in Hydraulically Fractured Wells With Pre-Existing Natural Fractures Using Unstructured Quadrilateral Grids. In SPE Asia Pacific Unconventional Resources Conference and Exhibition. Society of Petroleum Engineers.

Wang, J., & Rahman, S. S. (2016). Investigation of water leakoff considering the component variation and gas entrapment in shale during hydraulic-fracturing stimulation. SPE Reservoir Evaluation & Engineering, 19(03), 511-519.

Wang, C., Ran, Q., & Wu, Y. S. (2019). Robust implementations of the 3D-EDFM algorithm for reservoir simulation with complicated hydraulic fractures. Journal of Petroleum Science and Engineering, 181, 106229.

Warren, J. E., & Root, P. J. (1963). The behavior of naturally fractured reservoirs. Society of Petroleum Engineers Journal, 3(03), 245-255.

Williams, M. J., Khadhraoui, B., & Bradford, I. (2010). Quantitative interpretation of major planes from microseismic event locations with application in production prediction. In SEG Technical Program Expanded Abstracts 2010 (pp. 2085-2089). Society of Exploration Geophysicists.

Wu, K., & Olson, J. E. (2016). Numerical investigation of complex hydraulic-fracture development in naturally fractured reservoirs. SPE Production & Operations, 31(04), 300-309.

Xu, W., Le Calvez, J. H., & Thiercelin, M. J. (2009, January). Characterization of hydraulically-induced fracture network using treatment and microseismic data in a tight-gas sand formation: a geomechanical approach. In SPE tight gas completions conference. Society of Petroleum Engineers.

Xu, W., Thiercelin, M. J., Ganguly, U., Weng, X., Gu, H., Onda, H., ... & Le Calvez, J. (2010, January). Wiremesh: a novel shale fracturing simulator. In International oil and gas conference and exhibition in China. Society of Petroleum Engineers.

Xu, F., Yu, W., Li, X., Miao, J., Zhao, G., Sepehrnoori, K., ... & Wen, G. (2018, October). A fast EDFM method for production simulation of complex fractures in naturally fractured reservoirs. In SPE/AAPG Eastern Regional Meeting. Society of Petroleum Engineers.

Xu, Y., Cavalcante Filho, J. S., Yu, W., & Sepehrnoori, K. (2017). Discrete-fracture modeling of complex hydraulic-fracture geometries in reservoir simulators. SPE Reservoir Evaluation & Engineering, 20(02), 403-422.

Yaich, E., Williams, S., Goddard, P., de Souza, O. D., Bowser, A., & Foster, R. A. (2015, July). A case study: The impact of soaking on well performance in the Marcellus. In Unconventional Resources Technology Conference, San Antonio, Texas, 20-22 July 2015 (pp. 1911-1920). Society of Exploration Geophysicists, American Association of Petroleum Geologists, Society of Petroleum Engineers.

Yang, D., Xue, X., & Chen, J. (2018, April 22). High Resolution Hydraulic Fracture Network Modeling Using Flexible Dual Porosity Dual Permeability Framework. Society of Petroleum Engineers. SPE Western Regional Meeting, Garden Grove, California, USA, April 22-26.

Yan, Q., Lemanski, C., Karpyn, Z. T., & Ayala, L. F. (2015). Experimental investigation of shale gas production impairment due to fracturing fluid migration during shut-in time. Journal of Natural Gas Science and Engineering, 24, 99-105.

Yu, X., Rutledge, J., Leaney, S., & Maxwell, S. (2016). Discrete-fracture-network generation from microseismic data by use of moment-tensor-and event-location-constrained hough transforms. SPE Journal, 21(01), 221-232.

Yue, M., Leung, J. Y., & Dehghanpour, H. (2016). Numerical investigation of limitations and assumptions of analytical transient flow models in tight oil reservoirs. Journal of Natural Gas Science and Engineering, 30, 471-486.

Zhong, C., & Leung, J. Y. (2020). Numerical Analysis of the Effects of Apparent-Permeability Modeling and Secondary-Fracture Distribution for Hydraulic-Fractured Shale-Gas Production Analysis. SPE Reservoir Evaluation & Engineering.

Zhong, C., & Leung, J. Y. (2020). Numerical investigation of water retention in secondary fractures and apparent permeability modeling in shale gas production. Journal of Petroleum Science and Engineering, 107294.

Zhou, Q., Dilmore, R., Kleit, A., & Wang, J. Y. (2016). Evaluating fracture-fluid flowback in Marcellus using data-mining technologies. SPE Production & Operations, 31(02), 133-146.

Appendix A: Derivation of Permeability Tensor

Eq. (3.8) can be simplified to:

$$\boldsymbol{F} = \frac{1}{V}\Sigma_{m=1}^{M} A_m T_m \boldsymbol{n}_{im}\boldsymbol{n}_{jm}\boldsymbol{n}_{km}.$$

(A-1)

Next, the fracture tensor is projected to the x-, y-, and z-planes (Ghahfarokhi, 2017):

$$\boldsymbol{F} = \begin{bmatrix} F_{ii} & F_{ij} & F_{ik} \\ F_{ji} & F_{jj} & F_{jk} \\ F_{ki} & F_{kj} & F_{kk} \end{bmatrix},$$

(A-2)

$$F_{ii} = \frac{1}{V}\Sigma_{m=1}^{M} A_m e_m k_m \sin\left(Trend_m\right)\sin(Trend_m)$$

(A-3)

$$F_{jj} = \frac{1}{V}\Sigma_{m=1}^{M} A_m e_m k_m \cos\left(Trend_m\right)\cos(Trend_m)$$

(A-4)

$$F_{kk} = \frac{1}{V}\Sigma_{m=1}^{M} A_m e_m k_m \sin\left(Plunge_m\right)\sin(Plunge_m)$$

(A-5)

$$F_{ij} = F_{ji} = \frac{1}{V}\Sigma_{m=1}^{M} A_m e_m k_m \sin\left(Trend_m\right)\cos(Trend_m)$$

(A-6)

$$F_{ik} = F_{ki} = \frac{1}{V}\Sigma_{m=1}^{M} A_m e_m k_m \sin\left(Trend_m\right)\sin(Plunge_m)$$

(A-7)

$$F_{jk} = F_{kj} = \frac{1}{V}\Sigma_{m=1}^{M} A_m e_m k_m \cos\left(Trend_m\right)\sin(Plunge_m).$$

(A-8)

The trend angle is the clockwise angle between the fracture normal and the north; the plunge angle is the angle between the fracture normal and the x-y plane.

$$\boldsymbol{F}_{trace} = \begin{bmatrix} F_{11} & 0 & 0 \\ 0 & F_{22} & 0 \\ 0 & 0 & F_{33} \end{bmatrix},$$

(A-9)

$$F_{11} = F_{22} = F_{33} = F_{ii}\delta_{ii} + F_{jj}\delta_{jj} + F_{kk}\delta_{kk}$$

$$= \frac{1}{V}\Sigma_{m=1}^{M} A_m e_m k_m [\sin^2(Trend_m) + \cos^2(Trend_m) + \sin^2(Plunge_m)]. \tag{A-10}$$

The equivalent permeability tensor can be expressed as:

$$C_f = \frac{1}{V}\Sigma_{m=1}^{M} A_m e_m k_m, \tag{A-11}$$

$$\boldsymbol{k}_f = \lambda\left(\boldsymbol{F}_{trace}\delta_{ij} - \boldsymbol{F}\right) = \frac{1}{12}\begin{bmatrix} F_{11} & 0 & 0 \\ 0 & F_{22} & 0 \\ 0 & 0 & F_{33} \end{bmatrix} -$$

$$\frac{1}{12}\begin{bmatrix} C_f \sin(Trend_m)\sin(Trend_m) & C_f \sin(Trend_m)\cos(Trend_m) & C_f \sin(Trend_m)\sin(Plunge_m) \\ C_f \sin(Trend_m)\cos(Trend_m) & C_f \cos(Trend_m)\cos(Trend_m) & C_f \cos(Trend_m)\sin(Plunge_m) \\ C_f \sin(Trend_m)\sin(Plunge_m) & C_f \cos(Trend_m)\sin(Plunge_m) & C_f \sin(Plunge_m)\sin(Plunge_m) \end{bmatrix}. \tag{A-12}$$

$$\boldsymbol{k}_f = \frac{1}{12V}\sum_{m=1}^{M} A_e e_m k_m \left\{ \begin{bmatrix} C_{11} & 0 & 0 \\ 0 & C_{22} & 0 \\ 0 & 0 & C_{33} \end{bmatrix} - \right.$$

$$\left. - \begin{bmatrix} \sin(Trend_m)\sin(Trend_m) & \sin(Trend_m)\cos(Trend_m) & \sin(Trend_m)\sin(Plunge_m) \\ \sin(Trend_m)\cos(Trend_m) & \cos(Trend_m)\cos(Trend_m) & \cos(Trend_m)\sin(Plunge_m) \\ \sin(Trend_m)\sin(Plunge_m) & \cos(Trend_m)\sin(Plunge_m) & \sin(Plunge_m)\sin(Plunge_m) \end{bmatrix} \right\},$$

$$C_{11} = C_{22} = C_{33} = \sin^2(Trend_m) + \cos^2(Trend_m) + \sin^2(Plunge_m). \tag{A-13}$$

Appendix B: Calculation of Flowback Recovery

The flowback recovery(E) of the fracturing fluid is defined as the ratio of cumulative fracturing fluid production to the initial water in the fracturing system. The fracture-fluid volume in the main fracture is equal to 54.4 m^3. From Fig. 29(a), the water volume in the natural fracture can be read equal to 65 m^{3}for the original DPDK case and 96.6 m^{3}for the corrected DPDK case.

After three weeks of production, from Fig. 27(d), the cumulative water is equal to 78 m^3 for the original DPDK case and 90 m^3 for the corrected DPDK case. From Fig.29(b), the water produced from the matrix in the first three weeks after opening the well can be read equal to 72 m^3 same for the two cases. Therefore, in the case of the original DPDK, the produced water of the fracture system can be calculated as 6 m^3, and in the case of modified DPDK, it is 12 m^3. Finally, the flowback recovery of the fracturing fluid after three weeks of production can be calculated as:

$$E_{original} = \frac{6}{54.4+65} \times 100 = 5.06\%,$$

$$E_{corrected} = \frac{12}{54.4+96.6} \times 100 = 10.12\%.$$